



Available online at www.sciencedirect.com

ScienceDirect

Geochimica et Cosmochimica Acta 236 (2018) 99-120

Geochimica et Cosmochimica Acta

www.elsevier.com/locate/gca

Reverse weathering in marine sediments and the geochemical cycle of potassium in seawater: Insights from the K isotopic composition (⁴¹K/³⁹K) of deep-sea pore-fluids

Danielle P. Santiago Ramos ^{a,*}, Leah E. Morgan ^b, Nicholas S. Lloyd ^c, John A. Higgins ^a

^a Department of Geosciences, Princeton University, Princeton, NJ 08544, USA
 ^b U.S. Geological Survey, Denver, CO 80225, USA
 ^c Thermo Fisher Scientific, Bremen, Germany

Received 17 July 2017; accepted in revised form 21 February 2018; available online 2 March 2018

Abstract

In situ Al-silicate formation, also known as "reverse weathering," is an important sink of many of the major and minor cations in seawater (e.g. Mg, K, and Li). However, the importance of this sink in global geochemical cycles and isotopic budgets of these elements remains poorly constrained. Here, we report on the potassium isotopic composition (41 K/ 39 K) of deepsea sediment pore-fluids from four (Integrated) Ocean Drilling Program sites (1052, U1378, U1395 and U1403) to characterize potassium isotopic fractionation associated with the formation of authigenic Al-silicate minerals in marine sediments and its role in elevating the 41 K/ 39 K of seawater relative to bulk silicate Earth. Isotopic ratios are obtained by high-resolution multicollector inductively coupled plasma mass spectrometry (MC-ICP-MS) in cold plasma conditions with a long-term external reproducibility of ca. 0.17%. We find that, although all sites are characterized by pore-fluid K concentrations that decline with increasing depth, their K isotopic profiles vary systematically from site-to-site; at sites characterized by rapid sedimentation rates, pore-fluid profiles of 41 K/ 39 K are relatively invariant whereas at sites characterized by slow sedimentation rates, 41 K/ 39 K declines with depth by up to 1.8%. Results from 1-D diffusion-advection-reaction models suggest that these differences may result from a complex interplay between sedimentation rate and fractionation of K isotopes during diffusion, Al-silicate authigenesis, and ion exchange. Model simulations suggest fractionation factors between 0.9980 and 1.0000 for reverse weathering reactions in deep-sea sediments. Although deep-sea sites do not constitute major sinks of K in seawater, some of the processes responsible for K isotopic fractionation at these sites (diffusion and Al-silicate authigenesis) likely play a role in determining the 41 K/ 39 K of seawater.

© 2018 Elsevier Ltd. All rights reserved.

Keywords: Potassium cycle; Potassium isotopes; Al-silicate authigenesis; Reverse silicate weathering; Marine diagenesis; Pore-fluid chemistry; Ion exchange

1. INTRODUCTION

Feedbacks between climate, the global carbon cycle, and the chemistry of seawater stabilize Earth's surface temperature on geologic timescales and are likely responsible for its habitability over billions of years of Earth history (e.g. Walker et al., 1981; Berner et al., 1983). The most important component of the geologic carbon cycle is the precipitation and burial of carbonate sediments. The amount of carbonate sediment produced depends, in turn, on the alkalinity generated during silicate weathering less the amount consumed during the formation of secondary clay minerals both in terrestrial and marine systems (sediment and altered

^{*} Corresponding author.

E-mail address: dpramos@princeton.edu(D.P. Santiago Ramos).

oceanic crust). Mackenzie and Garrels (1966) first proposed that marine "reverse weathering" reactions consume alkalinity via the following simplified reaction between dissolved cations in seawater and Al-silicate minerals:

$$\begin{aligned} & \text{Al-silicate} + \text{SiO}_2 + \text{HCO}_3^- + (\text{Li}^+, \text{K}^+, \text{Mg}^{2+}) \\ &= (\text{Li}^+, \text{K}^+, \text{Mg}^{2+}) - \text{Al-silicate} + \text{CO}_2 + \text{H}_2\text{O} \end{aligned} \tag{1}$$

Because these reactions constitute a sink of seawater alkalinity but not CO₂, they act to offset alkalinity sources from continental silicate weathering. The net effect is that on timescales greater than the residence time of alkalinity in seawater (<10 kyr; Archer, 1991), changes in the alkalinity sink in marine Al-silicates will be balanced by changes in alkalinity sources from continental silicate weathering (Dunlea et al., 2017). Unfortunately, many aspects of marine Al-silicate authigenesis remain poorly constrained. In particular, little is known about rates of seawater potassium removal in authigenic marine Al-silicates or the role that this process may play in controlling the concentration of potassium in seawater on geologic timescales (e.g. Lowenstein et al., 2001; Hover et al.. Michalopoulos and Aller, 2004; Coogan and Gillis, 2013).

Recent advances in inductively coupled plasma massspectrometry now permit precise measurements of natural variability in the 41 K/39 K of terrestrial materials at the $\sim 0.1\%$ level. A major outcome of these new measurements is the discovery that seawater and bulk silicate Earth (BSE) have significantly distinct K isotopic compositions, as seawater has a δ^{41} K that is between 0.50 and 0.60% higher than BSE (Li et al., 2016; Wang and Jacobsen, 2016; Morgan et al., 2018). This difference indicates that there must be processes that fractionate K isotopes during either (1) continental silicate weathering and high-temperature basalt alteration (major seawater K sources-Kronberg, 1985; Spencer and Hardie, 1990; Demicco et al., 2005) or (2) formation of authigenic Al-silicates in marine sediments and low-temperature alteration of the oceanic crust (major seawater K sinks-Bloch and Bischoff, 1979; Staudigel and Hart, 1983; Kronberg, 1985; Elderfield et al., 1999; Wheat and Mottl, 2000).

In order to shed light on the processes that contribute to the elevated δ^{41} K value of seawater relative to bulk silicate Earth, we present the first K isotope measurements of deepsea pore-fluids from four sites (1052, U1378, U1395, U1403) drilled and sampled as part of the Ocean Drilling Program (ODP) and Integrated Ocean Drilling Program (IODP). Sites span a range of water depths, lithologies and sedimentation rates. However, pore-fluid profiles at all sites indicate overall declining K concentrations with depth, consistent with K removal by reactions within the sediment column and/or in the underlying oceanic crust. Despite their broadly similar K concentration profiles, the four studied sites are characterized by very different K isotope profiles. We also simulate each pore-fluid profile of K concentrations and isotopes using a 1-D sediment model that includes diffusion, reaction, and advection due to sediment compaction. We find that K isotope fractionation during diffusion, Al-silicate authigenesis, and ion exchange constitute reasonable mechanisms to explain the measured pore-fluid profiles, and that all sites can be simulated using a similar set of boundary conditions and model variables. Our results suggest that both diffusion in sedimentary pore-fluids and reverse weathering reactions fractionate K isotopes and likely play a role in elevating the ⁴¹K/³⁹K of seawater relative to bulk silicate Earth.

2. MATERIALS AND METHODS

2.1. Description of study sites

Pore-fluid samples are provided by the Integrated Ocean Drilling Program (IODP; U1378, U1395, and U1403) and by the Ocean Drilling Program (ODP; 1052). Locations include the North Atlantic Basin, with sites drilled in the J-Anomaly ridge (U1403) and the Blake Nose escarpment (1052), as well as the Caribbean Sea (U1395; Lesser Antilles Arc) and the North Pacific (U1378; Costa Rica margin). Studied sites span a range of water depths, ages and sediment compositions, and can be broadly classified into slow- (U1403, 1052) and fast-accumulating (U1395, U1378) sites (Table 1). Core recoveries were mostly good, allowing for predominantly continuous chemical records with depth; the exception is the interval between 125 and 177 meters below seafloor (mbsf) at Site U1395, where drilling difficulties led to poor core recovery and no pore-water samples (Fig. 1).

All sites are characterized by decreasing potassium concentrations with depth (Fig. 1), and show evidence of K uptake into secondary minerals during alteration of volcanic material within the sediment, in the underlying oceanic crust, or both. This conclusion is supported by negative correlations between pore-water Mg and Ca concentrations at Sites U1403 (Norris et al., 2014a) and 1052 (Norris et al., 1998a), an observation that is interpreted to reflect alteration of igneous material, as Ca²⁺ is released during weathering while Mg²⁺ is consumed (e.g. Gieskes, 1975, 1981). Declining pore-fluid ⁸⁷Sr/⁸⁶Sr values at U1378 (Supp. Table S1) provide additional evidence for alteration of volcanic material at this site (Ross et al., 2015). Given the short time span covered by sediments at U1378 (~1.5 Ma), variations in Sr isotopic ratios are too large to be attributed to changes in the composition of seawater and are better explained by mixing with less radiogenic Sr from igneous sources (Ross et al., 2015).

With the exception of U1403, where only one ash layer was identified (Norris et al., 2014a), all other study sites contain abundant volcanic material. Volcanogenic turbidites are a major component of the sediment pile in Site U1395 (Fig. 1C; Le Friant et al., 2013), while 82 tephra layers (felsic to mafic) were logged during drilling at U1378 (Vannucchi et al., 2012). At Site 1052, 9 ash layers were reported and dispersed volcanic material is common throughout the sediment column as are secondary alteration products such as authigenic (K-rich) glauconite, smectite, and zeolites (Norris et al., 1998a). The extreme thickness of the sediment column at this site (>5 km) indicates that alteration of the underlying oceanic crust is unlikely to be a major contributor to the pore-fluid K

Table 1 Site descriptions.

Expedition	Site	Hole	Coordinates	Depth	Drilled thickness (m)	Accumulation rates (cm/ky)	Age of drilled sediments	Simplified lithology	Depth of shallowest sample (mbsf)	Reported [K ⁺] of shallowest sample (mM)	Bottom- water temperature (°C)	Temperature gradient (°C/m)	Average bulk sediment density (g/cc)	Range of sediment porosity (%)	Notes:
171B	1052	A, E	29° 57.0906′N, 76° 37.5966′W	1344.5	684.8	1.8–2.6	Eocene to late Albian	Carbonate ooze and chalk with minor amounts of siliceous nannofossil ooze and zeolitic nannofossil chalk; abundant ash layers	7.95	12.6	3.59	0.0171	1.72	61.2–34.8	Temperature data from nearby site 1053
334	U1378	В	8° 35.5414/N, 84° 4.6306/W	526.7	523.9	23.6–51.6	Recent to late (?) Pliocene	Soft silty clay with sand (Pleistocene-Recent) to claystone/siltstone/sandstone (Pliocene-Pleistocene); abundant volcanic material	1.38	10.8	12.30	0.0514	2.69	72.5–54.6	
340	U1395	В	16°29.60/N, 61°57.09/W	1200.2	203.3	8–11	late to early Pleistocene	(Bio)volcaniclastic turbidites with variable amounts of hemipelagic sediment	4.40	10.8	5.15	0.0982	1.70	68.8–57.6	
342	U1403	A	39°56.60/N, 51°48.20/W	4944.3	253.3	0.13–1.56	Pleistocene to Campanian	Clay with nannofossils to radiolarian clay to nannofossil ooze with clay; mostly carbonate poor; one identified ash layer	14.75	12.3	2.46	0.0426	1.50	72.5–84.5	Temperature data from nearby site U1405

Data from site reports: 1052 (Norris et al., 1998a), U1378 (Vanucchi et al., 2012), U1395 (Le Friant et al., 2013) and U1403 (Norris et al., 2014a).

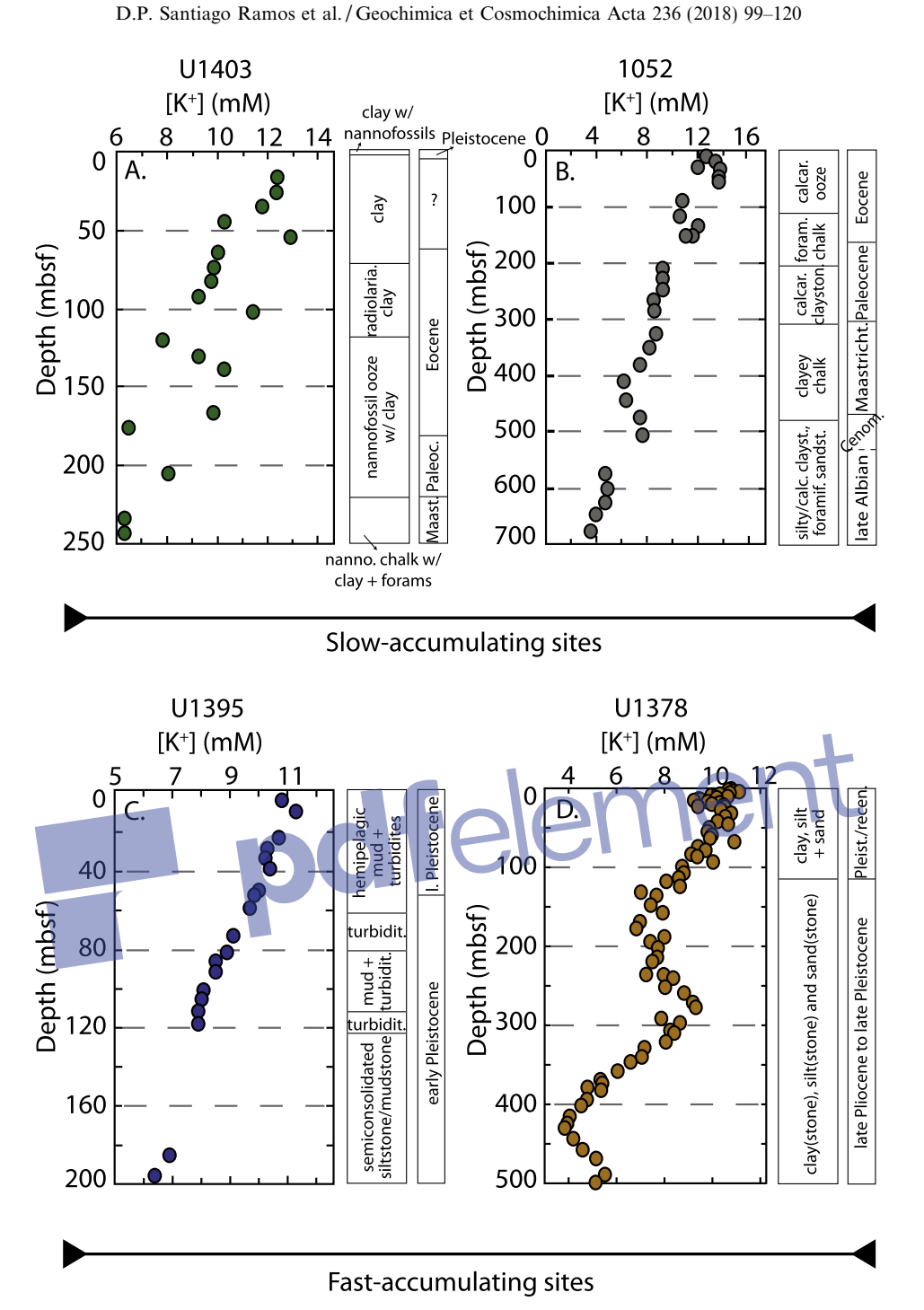


Fig. 1. Potassium concentration profiles for study sites. Depth is in meters below seafloor (mbsf) and 0 mbsf represents the sediment-water interface; stratigraphic columns are simplified versions of the lithologies observed at each site. Although rates of sediment accumulation vary across sites (see Table 1), all four profiles show decreasing K concentrations with depth. This is a common trend in many deep-sea sedimentary systems and is typically associated with K uptake during alteration of volcanic material within the sediment and/or in underlying oceanic crust. Chemical and sedimentological data sources: Norris et al. (1998a) (1052), Vannucchi et al. (2012) (U1378), Le Friant et al. (2013) (U1395), and Norris et al. (2014a) (U1403).

concentration profile. Rather, declining pore-fluid K concentrations at Site 1052 likely indicate formation of secondary Al-silicates during the alteration of volcanic material within the sediment column. Although there is little igneous material observed in the sediment column at Site U1403, there is abundant authigenic montmorillonite, a

hydrous clay that is capable of removing K from porefluid via sorption (Norris et al., 2014a).

Pore-fluid profiles of K concentrations at Sites U1403 and U1378 show considerable scatter (Fig. 1A and D; Vannucchi et al., 2012; Norris et al., 2014a) even when normalized to salinity (i.e. K/Cl). Possible explanations for this

include (1) artifacts during pore-fluid sampling (Mangelsdorf et al., 1969; Sayles and Manheim, 1975; de Lange et al., 1992; Sacchi et al., 2001), (2) external sources of fluid flow within the sediment column, and/or (3) reactions that lead to local net sources of K to the pore-fluid. The enriched K contents relative to seawater in the shallowest samples from Sites 1052 (12.6 mM) and U1403 (12.3 mM) are likely the result of sampling artifacts that have been observed in pore-fluid K concentrations since the early sampling missions (e.g. Mangelsdorf et al., 1969). External fluid flow is an unlikely explanation as geotherms for the studied and/or adjacent sites are linear with depth (Table 1: Norris et al., 1998b, 2014b; Manga et al., 2012; Vannucchi et al., 2012), and the sediment thickness and high siliciclastic content at Site U1403 preclude any significant convective flow in the sediment (McDuff, 1981). Finally, concomitant changes in K⁺ and NH₄ concentrations at Site U1378 suggest that ion-exchange reactions between sediment-bound K⁺ and pore-fluid NH₄ might be an important local source of K at this site (Vannucchi et al., 2012; Supp. Table S1). For example, K increases between $16-32 \text{ mbsf } (>1.5 \text{ mM}) \text{ and } 200-300 \text{ mbsf } (\sim 2 \text{ mM}) \text{ coin-}$ cide with NH₄⁺ increases of >4 mM and ~2 mM, respectively. NH₄ contents at U1378 are the highest observed across all study sites, with values of up to \sim 7 mM (Supp. Table S1). Ion-exchange reactions are also likely responsible for increasing Mg concentrations between 40 and 80 mbsf at Site U1395, which also coincide with increasing NH_4^+ contents of ~ 1 mM (Le Friant et al., 2013).

In this study, we chose to use paired K and Mg isotope analyses because Mg is affected by similar reactions as K and the isotopic effects of such reactions are relatively well known. For example, clay formation during alteration of volcanic material at low-temperatures is accompanied by positive fractionation factors, i.e. the Mg-mineral is enriched in the heavy ²⁶Mg isotope, leaving the residual pore-fluid Mg depleted in ²⁶Mg (Higgins and Schrag, 2010, 2015; Dunlea et al., 2017). The addition of Mg to

pore-fluids due to ion-exchange reactions with terrestrial clays has a similar effect on pore-fluid $\delta^{26} \text{Mg}$ values due to the light $\delta^{26} \text{Mg}$ composition of Mg bound in the interlayers of terrestrial clays (Wimpenny et al., 2014). Along with volcanic material alteration and ion-exchange reactions, pore-fluid Mg concentrations can also be affected by the formation of diagenetic carbonates, in particular dolomite. This complicates the interpretation of pore-fluid Mg isotope profiles. However, the Mg isotopic effects of dolomite formation are easily distinguishable from those associated with ion exchange or uptake into authigenic Al-silicates, as the relevant fractionation factors are opposite in sign (e.g. Higgins and Schrag, 2010, 2015). Authigenic dolomites are present in variable amounts at all sites, including the very carbonate-poor Site U1403.

2.2. Digestion of silicate standards

Six U.S. Geological Survey (USGS) igneous standards were also measured as part of this study to reproduce the results from Wang and Jacobsen (2016) and Li et al. (2016) and demonstrate that high-precision δ^{41} K values can be obtained by multi-collector mass spectrometry under cold plasma conditions. In addition, we also report the δ^{41} K values for two USGS shale samples (SBC-1 and SGR-1b; Table 2) and the first δ^{41} K measurements for three mineral standards from the Clay Minerals Society, which include one illite (Imt-2) and two smectites (SBId-1 and SWy-2). All of these whole-rock and mineral sample powders were digested at Princeton University using a MARS 6 microwave system. Prior to digestion, approximately 20 mg of powdered material was weighed into individual 100 mL PFA Teflon digestion vessels with trace-metal clean HF (40% v/v, 5 mL) and HNO₃ (70% v/v, 5 mL) and allowed to dissolve for 30 min under final temperature and pressure of 200 °C and 400psi. Solutions were then dried down for ~40 min under vacuum using a CEM Teflon evaporation system connected to the MARS 6 microwave. Finally,

Table 2 K isotopic composition of standards measured in this study.

External Standard Name	Standard ID	$\delta^{41}K_{BSW}~(\%o)$	n ⁱ	$2\sigma^{ii}$	SE ⁱⁱⁱ	Standard Source	
Guano Valley Andesite	AGV-2	-0.56	5	0.11	0.02	USGS	
Quartz Latite	QLO-1	-0.58	4	0.14	0.04	USGS	
Silver Plume Granodiorite	GSP-2	-0.48	3	0.11	0.03	USGS	
Columbia River Basalt	BCR-2	-0.55	4	0.13	0.03	USGS	
Hawaiian Basalt	BHVO-2	-0.52	2	0.24	0.08	USGS	
Centreville Diabase	W-2a	-0.55	2	0.21	0.08	USGS	
	Bulk Silicate Earth (BSE) average	-0.54	6	0.07	0.01		
Green River Shale	SGR-1b	-0.25	4	0.09	0.02	USGS	
Brush Creek Shale	SBC-1	-0.61	5	0.12	0.03	USGS	
Beidellite	Sp_Clay_SBId-1	-2.07	2	0.06	0.02	Clay Minerals Society	
Na-montmorillonite	Srce_Clay_SWy-2	-0.64	1	na	na	Clay Minerals Society	
Illite	Sp_Clay_Imt-2	-0.64	3	0.04	0.01	Clay Minerals Society	
Potassium Feldspar	SRM70b	-0.68	33	0.17	0.01	NIST	
Potassium Chloride	SRM999b	-0.03	55	0.17	0.01	NIST	
Bermuda Seawater	BSW	0.00	108	0.17	0.01	Collected in the field	

ⁱ n represents the number of full replicates (i.e. individual separates through column chemistry) analyzed on the MC-ICP-MS.

ii 2σ is calculated from all replicates. For n = 1, $2\sigma = 0.17\%$ (error on BSW).

iii Standard Error (SE).

3 mL of trace-metal clean HCl (36% v/v) were added to each vessel and a second digestion step of 30 min was performed (200 °C, 400psi). Digested samples were transferred into 15 mL PFA Teflon vials, allowed to dry overnight on a hotplate, and stored in 2% HNO₃ prior to column chemistry and mass-spectrometry analyses. Clay samples were not treated/purified prior to digestion and all acids used were distilled in-house.

2.3. Column chemistry

Chemical separation of cations for high-precision isotopic analyses by MC-ICP-MS was performed using an automated Dionex ICS-5000 + ion chromatography (IC) system at Princeton University (Fantle and Higgins. 2014; Blättler et al., 2015; Husson et al., 2015). Given the different amounts of material needed for K and Mg isotope measurements, chemical purification was performed in two individual steps. Pore-fluid samples were diluted to approximately 30 ppm K and 4 ppm Mg in 0.2% trace-metal grade HNO3 and loaded onto a Dionex CS-16 cation exchange column at a rate of 1 mL/min with methanesulfonic acid (MSA) as eluent. Minimum sample sizes needed for both column chemistry and massspectrometry were 6-7 ug of K and 0.5-1 ug of Mg, and samples were run along with external standards in order to monitor the efficacy of column chemistry. Potassium external standards included Bermuda seawater, two highpurity K solutions (KNO₃ from HPS and SRM 999b, a NIST KCl standard), and the NIST K-feldspar standard SRM 70b; for Mg runs, we used Cambridge-1 and Bermuda seawater as external standards. Purified K and Mg solutions were allowed to dry overnight in PFA Teflon vials, redissolved in 200 μL of 16 N (70% v/v) tracemetal grade HNO₃ in order to eliminate any organics, then dried again prior to isotopic analysis. To ensure purity, some of the separated potassium solutions were analyzed on a Thermo Scientific Element 2 inductively coupled plasma mass spectrometer (ICP-MS). The most "contaminated" separate had 6% magnesium relative to potassium, as well as lower amounts of Na, Ca, Al, Fe, Mn, and Sr. As will be further discussed below, this level of contamination does not affect the accuracy of our isotopic ratio analyses (Morgan et al., 2018).

2.4. Mass spectrometry

Purified K separates were diluted to 2 ppm K in 2% trace-metal grade HNO₃ prior to isotopic analysis on a Thermo Scientific Neptune Plus multi-collector inductively coupled plasma mass spectrometer (MC-ICP-MS) at Princeton University. Measurement of potassium isotopic ratios by MC-ICP-MS is hindered by the large isobaric interferences on masses 39 and 41, due to ionization of the carrier gas (argon) and formation of argon hydrides (³⁸ArH⁺ and ⁴⁰ArH⁺, respectively). Here, we use cold plasma (~600 W) settings and high mass-resolution mode (M/ΔM ca. 10,000; Morgan et al., 2018) to measure ⁴¹K/³⁹K ratios on small (2–3 milli-amu) but flat peak shoulders (Supp. Fig. S1).

The instrument was tuned to optimize stability and sensitivity, with 2 ppm K yielding voltages between 2 and 4 V on mass 39. Caution was taken to assure that samples matched standard concentrations (2 ppm K) to within 10% and the same batch of 2% HNO₃ was used to dilute both samples and standards in a single run. Instrumental mass-drift was taken into account by applying the standard-sample-standard bracketing technique with highpurity KNO₃ as the bracketing standard solution. As a test for data quality, a number of standards (also processed through column chemistry) were run along with unknowns, and sample δ^{41} K compositions were normalized to the average δ^{41} K of the seawater standard from the same analytical session. Normalized data are reported here as δ^{41} K, following the standard delta notation in permil (%):

$$\delta^{41}K = ((^{41}K/^{39}K)_{sample}/(^{41}K/^{39}K)_{standard} - 1) \times 1000$$
 (2)

Similar convention is used to report $\delta^{26} Mg$ values, although no normalization is applied for Mg isotope ratios. Our long-term external reproducibility of 0.17‰ (2σ , n = 108) for K isotope measurements is based on full sample replicates (i.e. including column chemistry) of the in-house Bermuda seawater standard (BSW, $\delta^{41} K \sim 0\%$). The K isotopic composition and long-term reproducibility of the remaining K standards can be found in Table 2.

Magnesium separates were diluted to 150 ppb and analyzed in low-resolution mode in the same Neptune MC-ICP-MS. Standard-sample-standard bracketing was also applied here, and measured Mg isotope ratios were plotted in 3-isotope space (26/24 Mg vs. 25/24 Mg; not shown) to verify that isotope variability was consistent with mass-dependent fractionation of Mg isotopes. The reported long-term external reproducibility for Mg measurements is the laboratory value of 0.09% (2 σ , n = 79; all measured at Princeton) and was derived from the isotopic offset of the Cambridge-1 standard (taken through column chemistry) against Dead Sea Magnesium (DSM-3). δ^{26} Mg values measured in this study for Cambridge-1 and seawater are -2.61 $\pm 0.02\%$ (2 σ , n = 2) and $-0.85 \pm 0.04\%$ (2 σ , n = 2), respectively, both indistinguishable from published values (Young and Galy, 2004). Reported errors on K and Mg isotopic measurements for each sample depend on the number of full replicates (i.e. number of chemical separations performed). We provide standard errors (2SE) for samples that have gone through column chemistry more than once. Otherwise, we report the external reproducibility on K $(2\sigma = 0.17\%)$ or Mg $(2\sigma = 0.09\%)$. For each run on the MC-ICP-MS, samples were analyzed in 2 or 3 blocks of 80 (for K) and 25 (for Mg) cycles. Internal errors for each block were $\leq 0.03\%$ and the 2σ error on the average δ^{41} K and δ^{26} Mg values from all blocks in a single run was typically ≤0.10%c.

2.5. Method validation for measurements of K isotopic ratios via MC-ICP-MS

Given the analytical challenges associated with isobaric interferences from ArH⁺ and the fact that K has only two abundant isotopes, we perform a series of tests to

characterize the accuracy of our measured $\delta^{41}K$ values, the dependence of measured $\delta^{41}K$ values on sample matrix, and whether our method can resolve mass-dependent fractionation of K isotopes (Morgan et al., 2018). Tests for reproducibility and precision follow the standard addition technique (e.g. Tipper et al., 2008)—where samples of different $\delta^{41}K$ values are mixed in known proportions prior to ion chromatography. Tests for matrix effects involve mixing synthetic matrix impurity solutions with K standards, and running these solutions against the pure K standard. Finally, we show that our method can accurately identify mass-dependent variations in $^{41}K/^{39}K$ ratios by intentionally fractionating potassium of a known isotopic composition during ion-exchange chromatography.

2.5.1. The standard addition technique

Based on the standard addition technique (Tipper et al., 2008), this experiment consisted in volumetrically mixing two end-members with different potassium isotope compositions and measuring the K isotopic ratio of the mixed solutions. The chosen end-member solutions were an evaporite (hanksite) with $\delta^{41}K = 0.43 \pm 0.10\%$, and a silicate (Kfeldspar) with $\delta^{41}K = -0.71 \pm 0.14\%$ (Morgan et al., 2018). Solutions were mixed by volume under known proportions and the expected K isotopic compositions of the final mixtures were calculated. Mixed solutions were then run through the ion-chromatography system for potassium purification, and the K isotopic ratios of the pure-K separates were measured on the MC-ICP-MS. Measured δ^{41} K values for the mixed solutions all fell within error ($2\sigma =$ 0.17%) of the expected two end-member mixing line, attesting to the accuracy of our methodology (Supp. Fig. S2).

2.5.2. Matrix effects in cold plasma MC-ICP-MS analyses of K isotope ratios

Precise and accurate measurements of K isotope ratios using MC-ICP-MS require purified K solutions to ensure that no other ionized species affect instrument fractionation—so-called matrix effects (e.g. Galy et al., 2001). Analytical advantages to measuring potassium isotopes under "cold plasma" conditions may exacerbate matrix effects—because a cooler plasma provides less ionization energy, the presence of matrix elements can lead to incomplete potassium ionization, thus promoting higher instrumental mass fractionation (Bryant et al., 2003).

As our most contaminated potassium separate had 6% Mg relative to K, we surveyed the matrix effect in our measurements by doping a K standard solution (OY-HPS, δ^{41} K = -0.13%, $2\sigma = 0.06\%$) with 6%, 8%, 10% and 20% magnesium relative to potassium (Morgan et al., 2018). Because Mg is not the only contaminant observed in K separates processed through the IC, these Mg-dominated matrix solutions also contained, in order of abundance: Na, Ca, Al, Fe, Mn and Sr (Supp. Table S2). The measured δ^{41} K for the contaminated solutions were all within error ($2\sigma = 0.06\%$) of the OY-HPS composition, although one can argue that the 20% Mg solution yielded statistically lower δ^{41} K values (Supp. Fig. S3). We believe, however, that our cation separation step does not yield such high

contamination levels and are confident that the presence of these contaminants in trace amounts is not likely to affect our measurements (Morgan et al., 2018).

2.5.3. Test for mass-dependent fractionation of K isotopes

To assess our ability to accurately measure massdependent fractionation on the MC-ICP-MS, we split the potassium peak from a NIST K standard solution (SRM 999b) into three fractions using the Dionex IC system (Morgan et al., 2018; Supp. Fig. S4). The analyzed fractions yielded δ^{41} K values that were high in the first cut, low in the second cut, and slightly lower in the third cut (Supp. Fig. S4). The weighted sum of all three fractions was indistinguishable from the δ^{41} K value of non-fractionated SRM 999b solution for all four experimental replicates (Supp. Table S2). These results followed a similar isotopic trend (high - intermediate - low) observed in an analogous experiment involving calcium (Supp. Fig. S4). In that case, fractionation on the column can be shown to be a massdependent process using a 3-isotope plot (e.g. $\delta^{44/42}$ Ca vs. $\delta^{43/42}$ Ca). The similarity of results from the Ca and K peak-splitting experiments indicates that the measured variability in δ^{41} K values is also mass-dependent (Morgan et al., 2018).

2.6. Description of numerical model

A 1-D diffusion-advection-reaction model is developed to simulate the observed potassium concentrations and measured isotopic compositions at each surveyed site. The main goal of our model simulations is to estimate the magnitude of K isotope fractionation associated with K cycling in deep-sea sedimentary environments. The model is constructed as a set of sediment boxes that accumulate and compact at a rate that is consistent with the age, thickness, and porosity of each site. At time steps when new sediment is added, the underlying sediment column is compacted following the porosity/depth relation from the individual sites (Richter and DePaolo, 1987, 1988), and the resulting loss of porosity is converted into pore-fluid that is advected upwards (towards the sediment-water interface). For time steps when no sediment is added, advection rates are zero.

Concentrations of ³⁹K and ⁴¹K in the pore-fluid are calculated simultaneously at each depth as the net result of transport fluxes (diffusion and advection) and reactions within the sediment, based on the following equation (e.g. Berner, 1980; Richter and DePaolo, 1987; Boudreau, 1997):

$$\phi(z) \cdot \frac{\partial^{n} K}{\partial t} = \frac{\partial (\phi(z) \cdot {}^{n} D(z) \cdot \frac{\partial^{n} K}{\partial z})}{\partial z} - \frac{\partial (\phi(z) \cdot \omega(z) \cdot {}^{n} K(z))}{\partial z} - \phi(z) \cdot {}^{n} R_{net}(z)$$
(3)

where z is depth below the sediment-water interface (m), t is time (y), ${}^{n}K$ (n = 39 or 41) is the depth- and time-dependent concentration of isotope ${}^{39}K$ or ${}^{41}K$ (mM), $\phi(z)$ and $\omega(z)$ are depth-dependent porosity (volume %) and advective flux (m/y), and ${}^{n}D(z)$ is the depth-dependent effective diffusion rate of isotope n (m²/y), which varies as a function of temperature and tortuosity of the sediment (Yuan-Hui and

Gregory, 1974; Boudreau, 1997). Both empirical observations and theoretical calculations indicate that K isotopes will diffuse at different rates in aqueous media (Bourg et al., 2010). To account for this, we use the relationship $^{41}D = \alpha_{diff}$. Where 0.9967 $\leq \alpha_{diff} \leq 0.9984$ (Bourg et al., 2010), in our model simulations.

The term ${}^{n}R_{net}(z)$ represents the net flux of ${}^{n}K$ into or out of the pore-fluid $(mM \cdot m^3 \cdot y^{-1})$ and may reflect the sum of two or more processes (e.g. secondary mineral formation, sorption onto mineral surfaces, and/or ion-exchange reactions). When K concentrations increase in the pore-fluids (e.g. U1378), this term is negative (K source); in contrast, when net K consumption is observed, ${}^{n}R_{net}(z)$ is positive (K sink). The presence of abundant volcanic material, negatively correlated Ca and Mg profiles, and/or authigenic silicate minerals in all sites suggests that reverse weathering of igneous material is most likely the main reaction leading to K uptake in these systems (see Section 2.1). In addition, reactions such as ion exchange (U1378 and U1395) and K sorption onto preexisting clays (U1403) might also be responsible for some of the observed variability in K concentrations with depth.

For both Sites U1403 and 1052, time-invariant and depth-dependent reaction rates are tuned to match reported K concentrations and measured K isotope profiles, and the same reaction rates are then applied for all subsequent model simulations. For the fast-accumulating sites (U1378 and U1395), we let reaction rates vary with time so as to simulate differences in sediment reactivity (e.g. from variable amounts of organic matter and volcanic ash) and/or the presence of transient local sources of K (e.g. through ion-exchange reactions between pore-fluid NH₄ and claybound K⁺; see Section 3.3.2). Finally, K isotopic fractionation associated with reactions within the sediment is defined by the general form of $\alpha_{reaction}$ according to the following equation:

$$\alpha_{reaction} = \frac{^{41}R_{net}}{^{39}R_{net}} \cdot \frac{^{39}K}{^{41}K} \tag{4}$$

where $\alpha_{reaction}$ might be associated with processes that consume K (α_{sink}) or lead to K increases in the pore-fluid (α_{source}). When the reaction term represents the net sum of two or more reactions, the fractionation factor is defined as α_{net} .

We solve Eq. (3) for both 39 K and 41 K by applying a finite difference scheme adapted for uneven grids in MATLAB (Pearson, 1968). Initial conditions are set to equal observed K concentrations from the shallowest sampled depth in each site (Table 1) and the δ^{41} K composition of seawater. It is important to note that initial K concentrations are typically higher than seawater due to artifacts associated with sampling and/or pore-water extraction from the sediments (Mangelsdorf et al., 1969; Sayles and Manheim, 1975; de Lange et al., 1992; Sacchi et al., 2001). However, despite higher-than-seawater K concentrations, measured K isotopic compositions for the shallowest sample at all sites are within error of the seawater value (δ^{41} K_{BSW} = 0 ± 0.17‰). The upper boundary condition (sediment-water interface) is defined as the history of

seawater K concentrations and δ^{41} K values over the time period corresponding to the age of the sampled sediment column. We assume both remain constant at the modern values (Lowenstein et al., 2001; Horita et al., 2002; Holland, 2005).

For the lower boundary condition, the shape of the concentration profile defines whether the flux is zero (no gradient) or constant (non-zero gradient). Since K concentrations continue to decrease with depth at all sites, we choose a constant flux type for our lower boundary (e.g. Boudreau, 1997), which is defined as the balance between K diffusion through this boundary and K consumption by reactions in the underlying sediment and/or oceanic crust. That is, although some pore-fluid profiles show evidence of oceanic crust alteration (see Section 2.1), we do not model this reaction explicitly. Instead, the lower boundary condition reflects the integrated effects of oceanic crust alteration as well as any reactions happening in the sediment below the cored intervals.

3. RESULTS

Pore-fluid profiles of K and Mg isotopes for all sites are shown in Table 3 and Figs. 2 and 3. Although all sites analyzed in this study are characterized by declining K concentrations with depth, measured δ^{41} K values yield two distinct isotopic profiles (Fig. 2). Notably, the two types of profiles broadly correlate with sedimentation rate. At sites with slow accumulation rates (U1403, 1052), pore-fluid δ^{41} K values decline with depth (Fig. 2A and B). For sites with fast sedimentation rates (U1395, U1378), pore-fluid δ^{41} K values deviate only slightly from the modern seawater value (δ^{41} K $_{BSW} \sim 0\%$; Fig. 2C-D).

3.1. Isotopic profiles at slow-accumulating sites

Measured δ^{41} K values for Site 1052 (Fig. 2B) range between -0.06% and -0.53% at 17.65 and 410.25 mbsf, respectively, and correlate with K concentrations ($r^2 = 0.794$; not shown). In contrast to the smooth depth-profile of K isotopes, Mg isotope trends at Site 1052 are more variable (Fig. 3B). In the upper ~ 150 meters of sediment, pore-fluids δ^{26} Mg values increase with depth by 0.50% (-0.81% to -0.31%), consistent with dolomite formation in the sediment column (δ^{26} Mg_{dol} $-\delta^{26}$ Mg_{fluid} < 0; Higgins and Schrag, 2010). For the interval between 150 and 207 mbsf, pore-fluid δ^{26} Mg values decline (-0.31% to -0.55%), and below 207 mbsf, δ^{26} Mg values increase slightly, reaching -0.39% at ~ 410 mbsf.

At U1403, measured δ^{41} K values (Fig. 2A) show an even larger range than Site 1052, with values between 0.08% (14.75 mbsf) and -1.72% (241.30 mbsf); here, too, K concentrations and K isotopic ratios are correlated ($r^2 = 0.785$; not shown). Our pore-fluid δ^{26} Mg values for U1403 do not show much variation and average at -0.64% ($2\sigma = 0.15\%$; Fig. 3A), slightly heavier than modern seawater (δ^{26} Mg_{BSW} = -0.80%; e.g. Higgins and

Table 3 Isotopic compositions of pore-fluid samples analyzed in this study.

Site and Hole	Core, section, interval (cm)	Depth (mbsf)	$\delta^{41}K_{BSW}$ (%)	ni	$2\sigma^{\mathrm{ii}}$	SE ⁱⁱⁱ	$\delta^{26/24} M g_{DSM}$ (%o)	$\delta^{25/24} M g_{DSM}$ (%o)	ni	$2\sigma^{ii}$	SE ⁱⁱⁱ
1052A	3H-3, 145–150	17.65	-0.06	3	0.18	0.05	-0.81	-0.41	1	0.09	
1052A	4H-3, 145–150	27.15	-0.06	3	0.16	0.03	-0.78	-0.41	1	0.09	
1052A	5H-3, 145–150	36.65	-0.11	2	0.06	0.02	-0.70	-0.36	1	0.09	
1052A	6H-3, 145–150	46.15	0.01	3	0.21	0.06	-0.64	-0.33	1	0.09	
1052A	7H-3, 145–150	55.65	0.01	3	0.18	0.05	-0.61	-0.33	1	0.09	
1052A	10H-3, 145-140	84.15	-0.10	3	0.23	0.07	-0.50	-0.26	1	0.09	
1052A	13H-3, 145-150	112.65	-0.12	3	0.24	0.07	-0.41	-0.23	1	0.09	
1052A	18X-3, 145-150	150.15	-0.20	3	0.05	0.02	-0.31	-0.20	1	0.09	
1052E	8R-2, 135-145	206.85	-0.41	2	0.08	0.03	-0.55	-0.34	1	0.09	
1052E	20R-3, 135-150	323.65	-0.53	3	0.12	0.04	-0.47	-0.23	1	0.09	
1052E	29R-3, 135–150	410.25	-0.53	2	0.26	0.09	-0.39	-0.22	1	0.09	
U1378B	1H-1, 138–150	1.38	-0.09	2	0.18	0.06	-0.79	-0.42	2	0.11	0.04
U1378B	2H-5, 138–150	12.68	0.07	1	0.17		-0.72	-0.39	1	0.09	
U1378B	3H-2, 138–150	17.68	-0.07	3	0.02	0.01	-0.67	-0.34	1	0.09	
U1378B	3H-6, 133–145	23.63	-0.04	1	0.17		-0.65	-0.33	1	0.09	
U1378B	5H-2, 138–150	36.68	-0.13	2	0.23	0.08	-0.13	-0.06	1	0.09	0.01
U1378B	7H-2, 138–150	55.68	0.01	1	0.17	0.01	-0.45	-0.23	2	0.01	0.01
U1378B	9H-2, 138–150	74.68	0.06	2	0.04	0.01	-0.49	-0.28	1	0.09	
U1378B	11H-3, 138–150	93.98	0.05	1	0.17		-0.42	-0.23	1	0.09	
U1378B	15H-,2 118–130	118.48 148.55	0.01 0.06	1 1	0.17 0.17		-0.28 -0.18	-0.15 -0.11	1 1	0.09 0.09	
U1378B U1378B	19X-5, 71–96 23X-6, 109–126	188.79	0.00	2	0.17	0.06	-0.18 -0.35	-0.11 -0.16	1	0.09	
U1378B	27X-2, 100–127	220.00	0.09	1	0.18	0.00	-0.56	-0.10 -0.29	1	0.09	
U1378B	31X-4, 118–150	252.48	-0.02	3	0.17	0.02	-0.30 -0.49	-0.29 -0.31	1	0.09	
U1378B	35X-5, 98–130	292.08	-0.01	1	0.17	0.02	-0.87	-0.48	1	0.09	
U1395B	1H-3, 140–150	4.40	-0.07	2	0.04	0.02	-0.81	-0.43	1	0.09	
U1395B	2H-3, 140-150	10.30	0.05	2	0.14	0.05	-0.83	-0.42	1	0.09	
U1395B	3H-5, 130-140	22.70	-0.06	2 3	0.08	0.02	-0.98	-0.51	1	0.09	
U1395B	4H-3, 140–150	29.32	-0.14	2	0.01	0.00	-1.05	-0.57	1	0.09	
U1395B	4H-6, 140–150	33.88	-0.17	2	0.10	0.04	-1.09	-0.59	1	0.09	
U1395B	5H-3, 140–150	38.80	-0.20	2	0.21	0.07	-1.15	-0.60	1	0.09	
U1395B	6H-4, 130–140	49.72	-0.17	3	0.13	0.04	-1.21	-0.63	1	0.09	
U1395B	6H-6, 140–150	52.85	-0.14	2	0.09	0.03	-1.26	-0.64	1	0.09	
U1395B	7H-4, 140–150	59.31	-0.22	3	0.11	0.03	-1.27	-0.63	1	0.09	
U1395B	9H-1, 140–150	72.60	-0.18	3	0.13	0.04	-1.27	-0.66	1	0.09	
U1395B	10H-2, 140–150	82.30	-0.06	3	0.21	0.06	-1.35	-0.70	1	0.09	
U1395B	10H-5, 140–150	86.81	-0.06	2	0.05	0.02	-1.31	-0.66	1	0.09	
U1395B	11H-3, 140–150	92.10	-0.02	2	0.10	0.04	-1.38 -1.27	-0.71	1	0.09	
U1395B U1395B	12H-3, 142–152 12H-6, 140–150	101.15 105.70	-0.04 -0.04	2 2	0.03 0.02	0.01 0.01	-1.27 -1.37	-0.64 -0.72	1 1	0.09 0.09	
				2						0.09	
U1395B U1395B	13H-4, 130–140 14H-3, 140–150	112.02 117.30	-0.03 -0.04	2	0.03 0.10	0.01 0.03	-1.26 -1.23	-0.67 -0.65	1 1	0.09	
U1395B	24X-1, 140–150	185.50	0.26	2	0.10	0.03	-1.23 -1.08	-0.58	1	0.09	
U1395B	25X-1, 140–150	195.10	0.20	2	0.07	0.02	-1.08 -1.09	-0.58 -0.58	1	0.09	
U1403A	2H-6, 145–150	14.75	0.08	3	0.45	0.13	-0.75	-0.39	1	0.09	
U1403A	3H-6, 145–150	24.25	-0.15	1	0.17						
U1403A	4H-6, 115-120	33.45	-0.11	1	0.17		-0.73	-0.37	1	0.09	
U1403A	7H-6, 145–150	62.25	-0.24	3	0.10	0.03	-0.67	-0.30	1	0.09	
U1403A	9H-6, 120–130	80.90	-0.55	1	0.17		-0.59	-0.29	1	0.09	
U1403A	10H-6, 140–150	90.61	-0.52	2	0.29	0.10					
U1403A	11H-6, 140–150	100.20	-0.50	2	0.23	0.08	-0.60	-0.32	1	0.09	
U1403A	14H-6, 136–146	128.54	-0.88	2	0.18	0.06	-0.59	-0.32	1	0.09	
U1403A	15H-5, 140–150	136.70	-0.95	3	0.22	0.06	-0.49	-0.26	1	0.09	
U1403A	19X-6, 120–130	164.70	-1.13	3	0.12	0.03	-0.63	-0.34	1	0.09	0.00
U1403A	20X-6, 130–140	174.50	-1.19	1	0.17	0.10	-0.61	-0.33	2	0.01	0.00
U1403A	23X-6, 130–140	203.40	-1.39	2	0.28	0.10	-0.63	-0.34	1	0.09	
U1403A U1403A	27X-5, 140–150 28X-5, 140–150	231.60	-1.46 -1.72	2 1	0.12 0.17	0.04	-0.69 -0.72	-0.34 -0.37	1	0.09 0.09	
	20 1- 3, 140-130	241.30	-1./2	1	U.1/		-0.72	-0.37	1	0.09	

i n represents the number of full replicates (i.e. individual separates through column chemistry) analyzed on the MC-ICP-MS. ii for $n=1,\,2\sigma$ is the long-term external reproducibility of BSW (K, $2\sigma=0.17~\%e$) or Cambridge-1 (Mg, $2\sigma=0.09\%e$). iii Standard Error (SE) is provided for samples with $n\geq 1$.

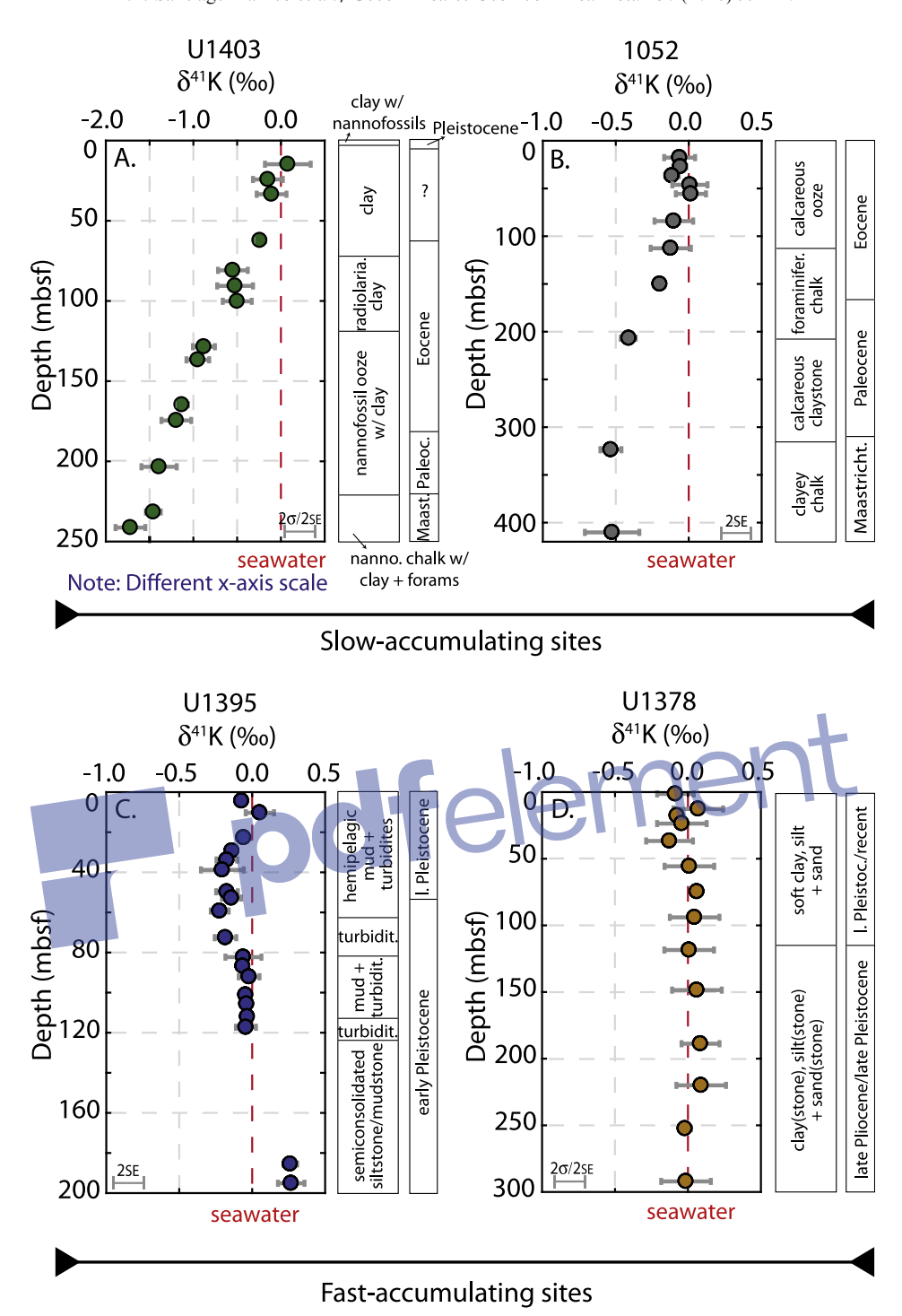


Fig. 2. Measured δ^{41} K values of deep-sea pore-fluids from Sites U1403 (A), 1052 (B), U1395 (C) and U1378 (D). These sediments can be subdivided into those with slow (A and B) and fast (C and D) accumulation rates based on the geometry of their isotopic profiles. Slow-accumulating sites show monotonic decrease in δ^{41} K values with depth, whereas fast-accumulating sites generally show δ^{41} K values close to seawater (red dashed line). For Sites 1052 (B) and U1395 (C), individual error bars represent measurement precision (2× standard error = 2SE) from full replicates of the same sample (i.e. multiple column chemistry separations). In the cases of U1403 (A) and U1378 (D), error bars represent 2SE for samples with n > 1 (Table 3); for samples with n = 1, the errors correspond to the long-term external reproducibility (2 σ) of 0.17% based on full replicates (n = 108) of our seawater standard. Sediment ages and simplified lithologies are based on data from site reports: Norris et al. (1998a) (1052), Vannucchi et al. (2012) (U1378), Le Friant et al. (2013) (U1395), and Norris et al. (2014a) (U1403). (For interpretation of the references to color in this figure legend, the reader is referred to the web version of this article.)

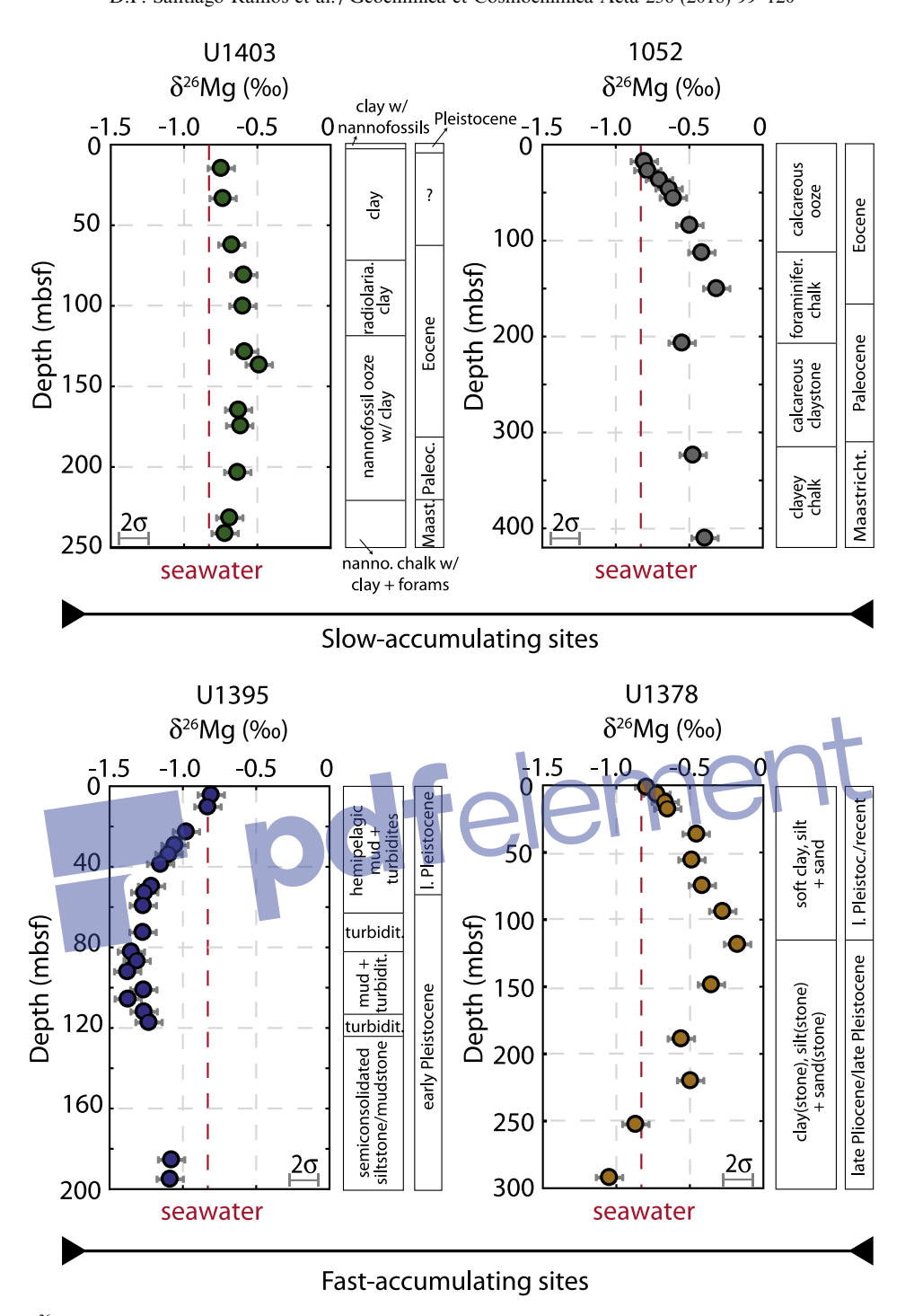


Fig. 3. Measured δ^{26} Mg values of pore-fluids with modern seawater Mg isotope composition for reference (red dashed line). Mg in marine pore-fluids is sensitive to the same reactions affecting K isotope profiles (e.g. reverse weathering and ion exchange) and can be used to aid in the interpretation of δ^{41} K variations with depth. δ^{26} Mg profiles show significant variability with depth for all sites with the exception of U1403. Individual error bars represent this laboratory's long-term external precision from full replicates of the Cambridge-1 standard ($2\sigma = 0.09\%$, n = 79). Sediment ages and simplified lithologies are based on data from site reports: Norris et al. (1998a) (1052), Vannucchi et al. (2012) (U1378), Le Friant et al. (2013) (U1395), and Norris et al. (2014a) (U1403). (For interpretation of the references to color in this figure legend, the reader is referred to the web version of this article.)

Schrag, 2010). Finally, we note that the decline in δ^{41} K values with depth at Site U1403 is considerably smoother than the K concentration profile. If the scatter in the concentration data is a result of sampling artifacts (e.g. de

Lange et al., 1992), our measurements indicate that any potential fractionation associated with these artifacts does not alter the pore-fluid δ^{41} K values at our current level of precision.

3.3. Model simulations

3.2. Isotopic profiles at fast-accumulating sites

While the depth profiles of δ^{41} K values at Sites 1052 and U1403 are characterized by monotonic decline, pore-fluid δ^{41} K profiles from Sites U1378 and U1395 remain moreor-less constant, with the exception of a short excursion to lower δ^{41} K values within the top tens of meters at U1395 (Fig. 2C). At this site, measured δ^{41} K values decrease from -0.07% at the sediment-water interface to -0.20% at 38.80 mbsf, recovering back to values of -0.02% at 92.10 mbsf (Fig. 2C). Between \sim 92 and 117 mbsf, δ^{41} K values remain constant and average -0.04% $(2\sigma = 0.02\%, n = 5)$. Measured δ^{26} Mg values decrease from -0.81% to -1.38% from 4.4 to 92.1 mbsf (Fig. 3C). The concomitant decrease in both K and Mg isotopic ratios, especially in the upper 60 meters of the sediment column, is also associated with an increase in pore-fluid NH₄ concentrations, from 0.01 to 1.05 mM (Supp. Table S1). In contrast with pore-fluids from the upper 117 meters of Site U1395, the two deepest samples are significantly enriched in ⁴¹K and average 0.26% ($2\sigma = 0.01\%$, n = 2). Largely due to poor core recovery, a 68-meter gap separates these deeper pore-fluid samples from the continuous record above. Pore-fluid chemistry is measurably different across the interval, with decreases in Mg (6.7 mM) and K (1 mM) and increase in Ca (3.4 mM), consistent with these deep samples having experienced additional alteration through reaction with igneous material in the sediment column.

Site U1378, our fastest accumulating site, has a rather scattered and complicated K concentration profile that is also reflected in the depth profiles of other cations (e.g. Ca²⁺, Mg²⁺, and NH₄; Supp. Table S1). Potassium correlates with Mg, Sr (both positively) and Ca (negatively), suggesting that all four cations are influenced by similar reactions (e.g. basalt alteration and associated authigenic Al-silicate formation). Pore-fluid samples from Site U1378 show an average δ^{41} K value of 0.01‰ ($2\sigma = 0.14$ ‰, n = 14; Fig. 2D), which is the same as the modern seawater K isotopic composition. However, δ^{41} K values reach as low as -0.13% at 36.38 mbsf, coinciding with an increase in NH_4^+ concentrations of ~ 4 mM. Also in this interval, K concentrations both increase and decrease, suggesting a complex interplay between sources and sinks of potassium. Rates of change in NH₄ concentrations also vary substantially below 36 mbsf: ammonium increases sharply between $50-94 \text{ mbsf } (\sim 3 \text{ mM}) \text{ and } 220-300 \text{ mbsf } (\sim 2 \text{ mM}), \text{ and }$ slowly decreases from 94 to 220 mbsf. Unlike Site U1395, the Mg isotopic composition of these pore-fluids appears to be controlled by the formation of authigenic dolomite in the upper 150 meters of the sediment column, as porefluid $\delta^{26} Mg$ values increase from -0.79% to -0.18%(Fig. 3D). Below 150 mbsf, δ^{26} Mg values decline back to near modern seawater values (-0.87% at 292 mbsf). Finally, there is a negative correlation ($r^2 = 0.604$; not shown) between pore-fluid δ^{41} K values and 87 Sr/ 86 Sr ratios (Ross et al., 2015), further suggesting that both isotope systems are being affected by similar processes (see Section 2.1).

Model simulations are used to assess the relative roles of diffusion, reverse weathering and other reactions (e.g. ion exchange and K sorption onto clays) in setting the pore-fluid δ^{41} K profiles at each site. The initial step is to specify net reaction rates that reproduce the individual K concentration profiles. Positive net reaction terms represent net K sinks and decreasing K concentrations, whereas negative net reaction rates are associated with net increases in K concentrations due to local K sources (Supp. Figs. S5 and S6). Next, we explore the relative importance of diffusion and reaction on determining the shape of the pore-fluid δ^{41} K profiles. First, we assume that the only process leading to K isotopic fractionation is diffusion. Second, we simulate δ^{41} K profiles with K fractionations associated with both aqueous K diffusion and K-consuming reactions. In this scenario, sink reactions are assumed to be (1) the formation of secondary Al-silicates during alteration of volcanic material (1052, U1378, U1395) and (2) K sorption onto montmorillonite (U1403). Finally, we consider more complex reaction terms that include time-dependent reaction rates and local K sources.

3.3.1. Assessing isotopic fractionation due to aqueous K diffusion and K-consuming reactions

In simulations where diffusion is assumed to be the only process fractionating pore-fluid K isotopes, we find that the range of α_{diff} values suggested by Bourg et al. (2010) is sufficient to explain the K isotopic trends from sites with slow accumulation rates (U1403 and 1052; Fig. 4A and B). However, at the fast-accumulating Sites U1395 and U1378 (Fig. 4C and D), measured δ^{41} K values do not agree with model outputs. These results suggest that chemical diffusion of K through the pore-fluid is a reasonable mechanism to explain most of the variability observed in the δ^{41} K and K concentration profiles at the slow-accumulating sites but not at fast-accumulating sites. At these, model outputs that include only K fractionation during diffusion produce δ^{41} K values that are too low at depth in the sediment column (Fig. 4C and D). Additional processes that fractionate K isotopes are needed to fully explain these profiles.

One possibility is fractionation of K isotopes during reactions that consume pore-fluid K. To simulate this scenario, we assume that reactions responsible for K uptake are associated with fractionation factors (α_{sink}) ranging between 0.9990 and 1.0000. Model results for these simulations are shown in Fig. 5. In this second scenario, model outputs are closer to explaining the K isotopic profiles observed at the fast-accumulating Sites U1395 and U1378 (Fig. 5C and D). Note that this scenario makes no attempt at reproducing the local deflections in the K concentrations reported for Site U1378 (Supp. Fig. S5-D). δ^{41} K profiles for Sites 1052 and U1403 are still well-matched under this scenario (Fig. 5A and B), provided that α_{diff} factors are adjusted accordingly (Table 4). That is, since pore-fluids are left enriched in ${}^{41}K$ for $\alpha_{sink} < 1.0000$, a larger fractionation factor for K isotope fractionation during diffusion is needed to produce good model fits. For Site U1403, we find

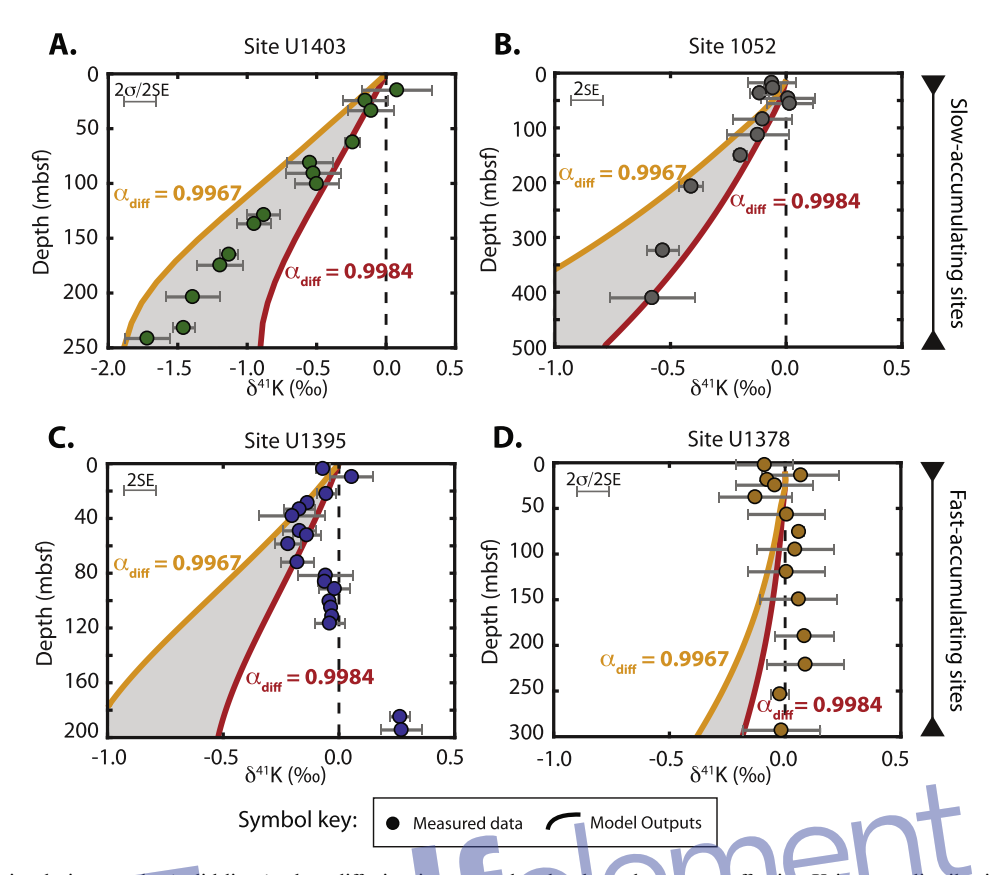


Fig. 4. Model simulation results (solid lines) when diffusion is assumed to be the only process affecting K isotope distribution between fluid and solid phases. The range of α_{diff} suggested in Bourg et al. (2010), 0.9967–0.9984, is sufficient to explain the trends in measured K isotopic values (solid circles) from slow-accumulating Sites U1403 (A) and 1052 (B). Fast-accumulating sites, however, are not well matched by model results, as is the case for U1395 (C) and U1378 (D). In the latter case, estimated pore-fluid δ^{41} K values become too light at depth. Black dashed lines represent the seawater δ^{41} K value. K concentration profiles for these model simulations are shown in Supplementary Fig. S5.

that the estimated K isotopic fractionation during reaction (α_{sink}) is the smallest across all sites, nearing 1.0000 for an α_{diff} of 0.9974. This result suggests that K uptake in these sediments, which includes K sorption onto hydrous clays, is likely not accompanied by any significant fractionation of K isotopes. We keep α_{diff} equal to 0.9974 for all sites in the following simulations.

3.3.2. Potential isotope effects on pore-fluid potassium during ion exchange

Although a model scenario that includes K isotope fractionation during both diffusion and K-consuming reactions improves our model fits for the fast-accumulating sites, it captures neither the light δ^{41} K values observed in the upper few tens of meters at both U1378 and U1395, nor the enriched values at depth in Site U1395 (Fig. 5C-D). In order to reproduce these aspects of the pore-fluid δ^{41} K profiles, we must change our model in two ways.

First, we assume that the various diagenetic reactions are time-dependent. Reaction rates are set to vary at specific times during sediment deposition (Table 4), which follows site-specific accumulation rates. We do this to explore the possibility that changes in sediment composition with time will lead to layers (boxes) with different

reaction rates (in sign and/or magnitude). This assumption is grounded in observations from site reports that organic carbon and volcanic material contents are variable with depth. These variations in composition might be important because organic matter degradation can source NH₄⁺ for ion-exchange reactions with K⁺, while alteration of volcanic material is a sink of K in these systems.

Second, we assume that there are additional reactions involved in the cycling of K through the pore-fluid. One possibility is ion exchange between NH₄ in the pore-fluid and K⁺ in the interlayers of detrital clay minerals (a K source). Evidence for this process at Sites U1378 and U1395 includes (1) the occurrence of low δ^{41} K values in depth intervals associated with rapid increases in porefluid NH⁺ concentrations in both sites (e.g. upper ~40 meters of sediment in U1378 and U1395) and (2) the observation at Site U1395 of an increase in pore-fluid Mg concentrations and a decline in δ^{26} Mg values within the same depth interval corresponding to a δ^{41} K negative excursion. Although cycling of Mg in the pore-fluid may also involve multiple reactions (e.g. dolomitization, ion exchange, reverse weathering; Higgins and Schrag, 2010), the lowest pore-fluid δ^{26} Mg value from U1395, -1.27% at ~ 60 mbsf,

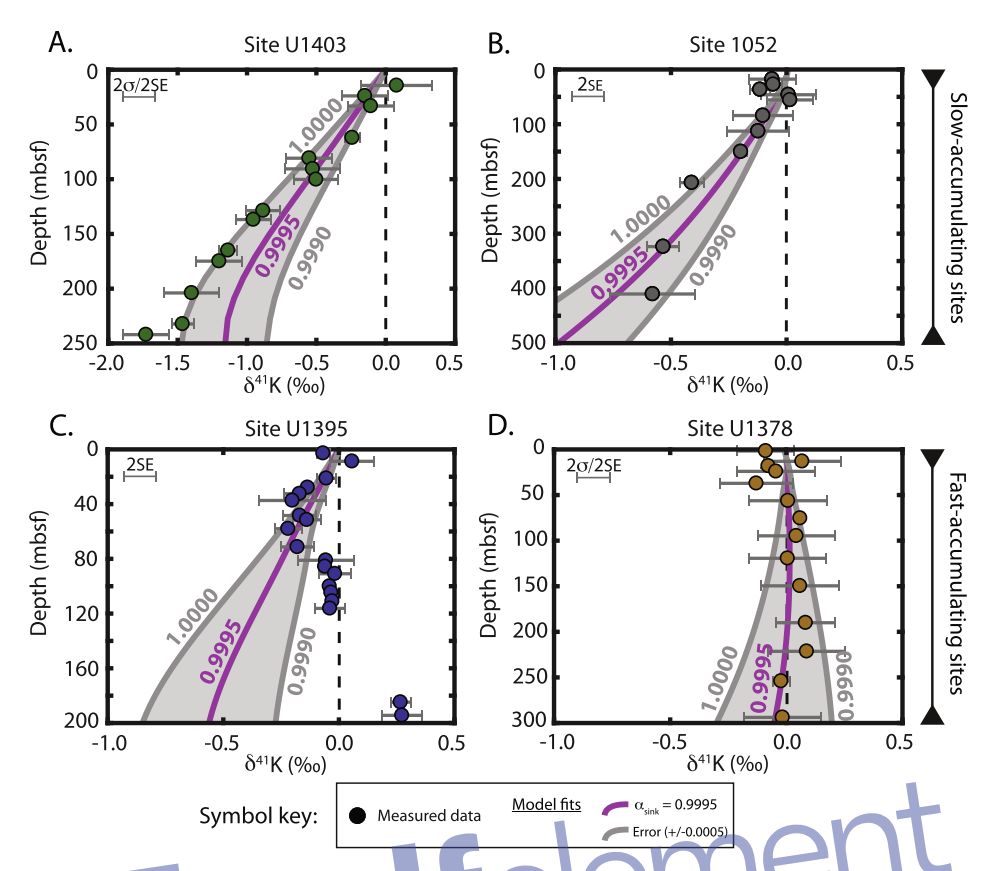


Fig. 5. Model simulation results (solid lines) when both diffusion and K-consuming reactions lead to K isotope fractionation in the porefluids. For this scenario, we choose a single α_{diff} value for all sites (0.9974) and consider a range of K isotope fractionations associated with reactions that may consume K (α_{sinik} between 0.9990 and 1.0000). At Site U1403 (A), α_{sinik} appears to be close to 1.0000, suggesting that K uptake in these sediments is likely not associated with any significant isotope effect. For all other sites, $\alpha_{sinik} < 1.0000$ is required to reproduce some or all variability in measured δ^{41} K values. The improved model results for Sites U1395 (C) and U1378 (D) indicate that reaction plays an important role in the K isotope cycling in these sediments. Black dashed lines represent the seawater δ^{41} K value. K concentration profiles for these model simulations are shown in Supplementary Fig. S5.

is consistent with a local, isotopically light Mg source. Indeed, estimates of the δ^{26} Mg value of interlayer Mg in terrestrial clays is $\sim -1.31\%$ (Wimpenny et al., 2014).

The effect of adding a local K source to the model (e.g. from ion-exchange reactions) can be described using the following isotope mass-balance equation:

$$\varepsilon_{source} = \frac{R_{sink}}{R_{source}} \cdot (\delta^{41} K_{fluid} + \varepsilon_{sink}) \\
- \frac{R_{net}}{R_{source}} \cdot (\delta^{41} K_{fluid} + \varepsilon_{net}) - \delta^{41} K_{source} \tag{5}$$

where the subscripts $_{sink}$, $_{source}$ and $_{net}$ refer to pore-fluid K consumption via reverse weathering, pore-fluid K production due to ion exchange, and net flux of K into or out of the pore-fluid, respectively; R corresponds to gross or net reaction rates and R_{net} can either be positive ($R_{sink} > R_{source}$) or negative ($R_{source} > R_{sink}$); ε is the individual or net fractionation factor associated with K cycling reactions and relates to α by the equation ε (‰) = $(\alpha - 1) \cdot 1000$; $\delta^{41} K_{fluid}$ is the average $\delta^{41} K$ value of the local pore-fluid; and, lastly, $\delta^{41} K_{source}$ is the isotopic composition of the local K source, which we assume to be BSE-

like with $\delta^{41}K = -0.54\%$, as the bulk of the Al-silicate fraction in these sites is of detrital origin.

Fig. 6A shows model results for Site U1395, where we have assumed (1) higher net reaction rate (2 times faster) for sediment boxes between ~21-63 mbsf and (2) net K isotopic fractionation (α_{net}) of 1.0008 for that depth interval. Note that model fits that successfully reproduce the heavy δ^{41} K values at depth require larger α_{sink} values between 0.9980 and 0.9985. Here, the estimated α_{net} can be reconciled with net reverse weathering reactions (i.e. $R_{sink} > R_{source}$) with an α_{sink} of 0.9985 if the process responsible for local K release is accompanied by isotopic fractionations (ε_{source}) greater than -1.17% (Fig. 7). As previously discussed, ion exchange between clay-bound K⁺ and pore-fluid NH₄⁺ is a plausible mechanism to explain these local K-sourcing reactions; however, since the fluxes of K associated with this process are small compared to the reservoir of potential exchangeable K in the sediments, such large isotopic effects are not expected to lead to significant changes in the δ^{41} K value of the bulk sediment.

Fig. 6B shows model results for Site U1378. Output simulations are considerably improved when we reproduce the

Table 4
Parameters for model simulations.

Study site	R _{net w/in colum}	$_{nn}$ (mM·m ³ /y)	$R_{net\ at\ LB}\ (mM\cdot m^3/y)$		α_{diff}	$\alpha_{reaction}$	
1. Isotope fr	actionation during diffusion	n (depth-dependent, time inv	variant reactions; $LB = lov$	ver bounda	ry)		
1052	7.00E-10		7.00E-10		0.9967-0.9984	1.0000	
U1378	6.60E - 09		6.60E - 09		0.9967-0.9984	1.0000	
U1395	9.00E-09		9.00E-09		0.9967-0.9984	1.0000	
U1403	4.50E-09		7.00E-09		0.9967-0.9984	1.0000	
Study site	R _{net w/in colum}	$_{nn}$ (mM·m ³ /y)	$R_{net~at~LB}~(mM\cdot m^3/y)$		α_{diff}	α_{sink}	
2. Isotope fr	actionation during diffusion	n and clay formation (depth	-dependent, time invariant	reactions)		_	
1052	7.00E-10		7.00E-10		0.9974	0.9990 - 1.0000	
U1378	6.60E - 09		6.60E - 09		0.9974	0.9990 - 1.0000	
U1395	9.00E-09		9.00E-09		0.9974	0.9990 - 1.0000	
U1403	4.50E-09		7.00E-09		0.9974	0.9990-1.0000	
Study site	Simulation time (y) ⁱ	$R_{\textit{net w/in column}} \; (mM{\cdot}m^3\!/y)$	$R_{net\ at\ LB}\ (mM\cdot m^3/y)$	α_{diff}	α_{net}	α_{sink}	
3. Isotope fr	actionation during diffusion	n, Al-silicate formation and	local K-sourcing reactions	(time-depe	endent reactions)		
U1378	0-204,800	-5.00E-10	8.00E-10	0.9974	Unconstrained ⁱⁱ	Unconstrainedii	
	204,800-389, 120	2.50E-08	8.00E-10	0.9974	Unconstrained ⁱⁱ	Unconstrainedii	
	389,120-942,080	5.00E + 10	8.00E-10	0.9974	1.0060	0.9985	
	942,080-1,392,640	1.60E-08	8.00E-10	0.9974	0.9989	0.9985	
	1,392,640-1,433,600	-1.00E-07	8.00E-10	0.9974	0.9998	0.9985	
	1,433,600-1,500,040	2.75E-07	8.00E-10	0.9974	1.0004	0.9985	
U1395	0-1,536,000	9.00E-09	5.00E-09	0.9974	0.9980-0.9985	0.9980-0.9985	
	1,536,000–1,945,600 1.80E–08		5.00E-09	0.9974	1.0008	0.9985	
	1,945,600-2,100,400	9.00E-09	5.00E-09	0.9974	0.9980-0.9985	0.9980-0.9985	

ⁱ Simulations start at t = 0 and end at t = age of oldest sediment.

ii We do not attempt to constrain K isotope fractionation during reaction for depth intervals from which no pore-fluid sample was obtained.

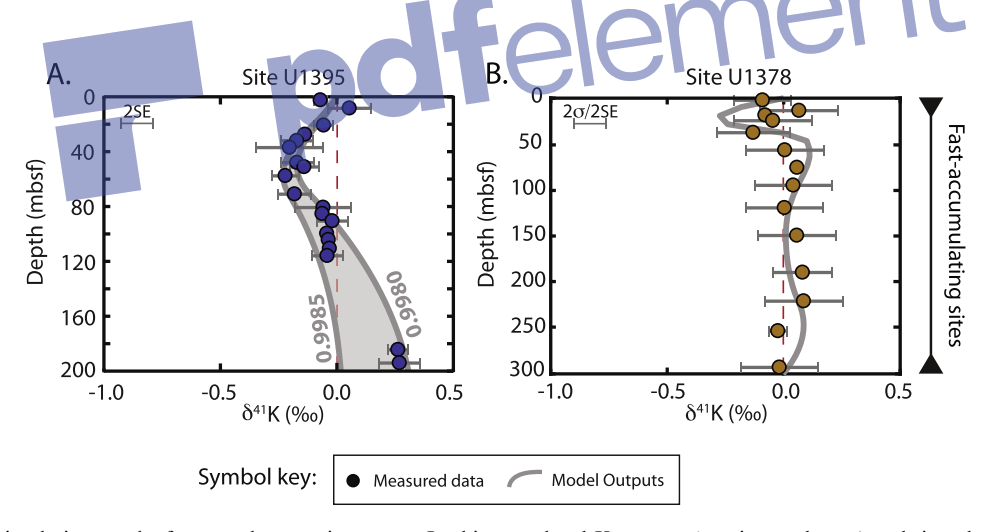


Fig. 6. Model simulation results for complex reaction terms. In this case, local K sources (e.g. ion exchange) and time-dependent reaction rates have been used to capture the negative values observed at the upper few tens of meters in Sites U1395 (A) and U1378 (B). These more negative values in both Sites U1395 and U1378 could be the result of the preferential release of 39 K into the pore-fluid from the interlayers of non-swelling clays (e.g. illites). Fractionation during K release is likely due to kinetic isotope effects associated with diffusion-controlled K transport from the interlayer sites of non-hydrated Al-silicates. Red dashed lines represent the seawater δ^{41} K value. K concentration profiles for these model simulations are shown in Supplementary Fig. S6. (For interpretation of the references to color in this figure legend, the reader is referred to the web version of this article.)

variable K concentration profile reported for this site (Fig. S6-B) in addition to considering the effects of diffusion and reaction. In this simulation, net reaction rates vary with time in order to match the shifting balance between K consumption and local K sources (Table 4; Supp. Fig. S6-B). Specifically, the increase in K concentration around

37 mbsf is simulated with a negative reaction rate (net K source) and coincides with the lightest measured δ^{41} K value of -0.13% for an $\alpha_{net} = 0.9998$. The association of light δ^{41} K values with increasing pore-fluid NH₄⁺ concentrations, and the overall high NH₄⁺ content of these fluids (Supp. Table S1) both suggest that ion-exchange reactions are

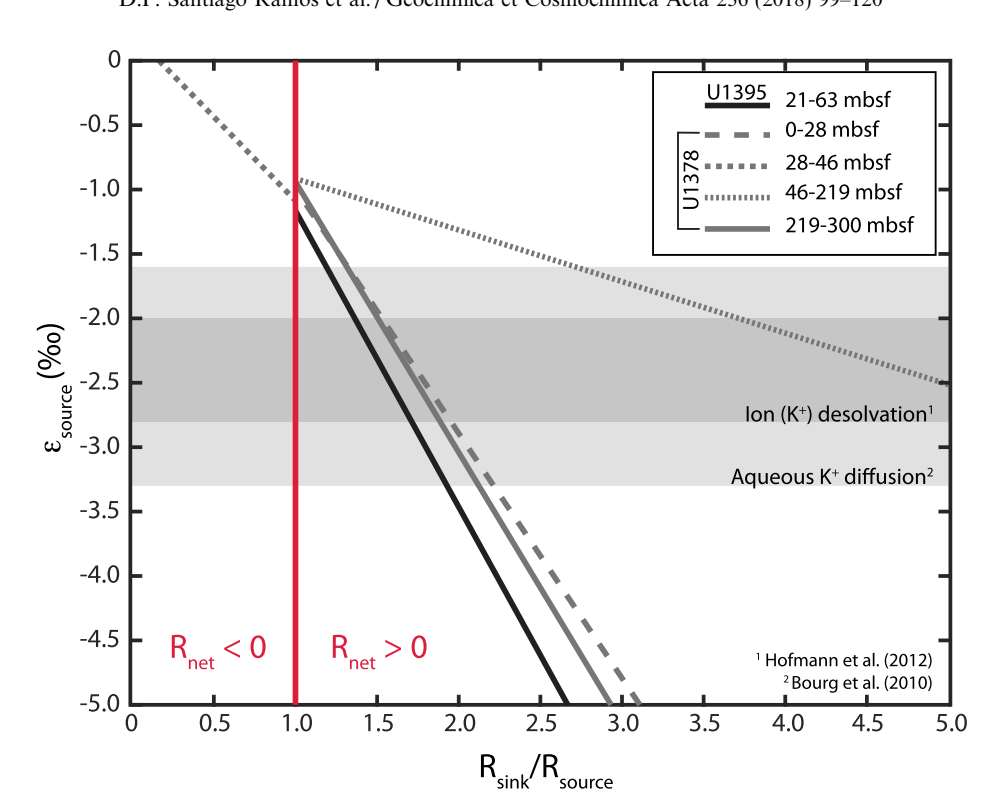


Fig. 7. Estimated K isotope effects due to K-sourcing reactions in pore-fluids from Sites U1378 and U1395. Plotted here are the K isotope fractionations (ε_{source}) associated with local pore-fluid K sources as a function of the relative gross rates of K consumption and production (R_{sink}/R_{source}); α_{sink} is set at 0.9985 and the δ^{41} K-source is assumed to have a BSE-like value of -0.54%c. The solid red line sets the boundary between regions of net K source ($R_{net} < 0$; 28–46 mbsf at U1378) and net K sink ($R_{net} > 0$; all other intervals) reactions. Calculated ε_{source} values vary widely due to our poor constraints on gross rates of reaction. Smaller fractionations are expected for cases when $R_{sink} \sim R_{source}$ or when $R_{source} > R_{sink}$; in contrast, for cases when $R_{sink} \gg R_{source}$, the ε_{source} values needed to explain the isotopic profiles at Sites U1395 and U1378 can be significantly large. Note that some of these larger estimates of ε_{source} are comparable in magnitude to other reported kinetic isotopic effects, such as those during aqueous K diffusion (light gray shaded area; Bourg et al. (2010)) and ion desolvation (dark gray shaded area; Hofmann et al. (2012)).

involved in the local K cycling. Although the pore-fluid δ^{41} K profile for Site U1378 shows virtually no variation, it does not mean that K cycling reactions are unimportant here. In fact, to achieve model outputs that provide good fits to the data requires net reaction terms with fractionation factors that offset the isotopic effects associated with aqueous diffusion. α_{net} values are thus tuned to reproduce the overall flat K isotopic profile observed at Site U1378 and vary for different depth intervals $(0.9989 \leq \alpha_{net} \leq 1.0060; \text{Table 4})$.

We can again use Eq. (5) to assess potential isotopic effects associated with K cycling at this site. In this case, we are interested in the trade-offs associated with including K-sourcing reactions such as ion exchange. For all intervals where net reaction rates are positive (i.e. where K consumption via reverse weathering is the likely dominant reaction), estimated α_{net} values are consistent with an $\alpha_{sink} = 0.9985$ when K-sourcing reactions are accompanied by fractionation factors (ε_{source}) that are <-0.90 to -1.00 for all depths (Fig. 7). Similar to U1395, these estimated fractionation factors are consistent with the preferential release of the light isotope of potassium during exchange with porefluid NH₄⁺. Finally, for the interval in U1378 where $R_{net} < 0$ (28–46 mbsf), calculated ε_{source} values are indistin-

guishable from fractionations estimated for the other intervals (\sim -1.00%) if the gross rates of K consumption are just slightly smaller than the gross production rates (i.e. $R_{sink}/R_{source} \approx 1$; Fig. 7). Because gross rates for R_{sink} and R_{source} are unknown at these sites, we cannot place strong constraints on ε_{source} associated with ion exchange in these pore-fluids. However, in cases when rates of K release are small relative to R_{sink} (i.e. $R_{sink}/R_{source}\gg 1$), much larger fractionation factors are needed in order to fit the low δ^{41} K values at U1395 (Fig. 7). These larger isotope effects would be in some cases comparable to those predicted from other kinetically controlled processes, such as aqueous diffusion (-1.6% to -3.3%; Bourg et al., 2010) and ion desolvation (-2.0% to -2.8%; Hofmann et al., 2012).

4. DISCUSSION

The results presented here bring new insights into the processes that may lead to K isotope variability in low-temperature systems and contribute to modern seawater being ~0.50% enriched in ⁴¹K relative to bulk silicate Earth. First, our results support laboratory estimates of K isotope fractionation during aqueous diffusion (Bourg et al., 2010) and show that diffusive K fractionation plays

115

an important role in determining the δ^{41} K value of deep-sea pore-fluids and authigenic marine silicates. Second, we provide the first constraints on K isotope fractionation during reverse silicate weathering in marine sediments. Our results indicate that ⁴¹K is variably depleted in secondary silicates, with fractionation factors ranging from 0.9980 to 1.0000 and larger magnitude isotope effects likely resulting from formation of anhydrous clay and/or faster rates of authigenic mineral formation. Third, the association between local increases in K concentrations and light measured δ^{41} K values (e.g. U1378) might be a result of reactions leading to the preferential release of ³⁹K into the pore-fluids. Although further studies are required, one possible explanation is NH₄⁺-for-K⁺ ion exchange with detrital or secondary clays accompanied by kinetic isotope effects during diffusion-controlled K transport from the mineral interlayer (Ruiz Pestana et al., 2016).

4.1. Fractionation of K isotopes by chemical diffusion in deep-sea pore-fluids

Experimental results and molecular dynamic (MD) simulations at infinite dilution show that potassium isotopes are fractionated during aqueous diffusion, with α_{diff} estimated to be between 0.9967 and 0.9984 (Bourg et al., 2010). Although aqueous diffusion in deep-sea sediments is affected by higher salinity, sediment tortuosity and changes in porosity with depth, the same range of fractionation factors predicted for aqueous diffusion are needed to explain the δ^{41} K profiles at Sites 1052 and U1403. Arguably, a narrower range of 0.9967-0.9974 is sufficient to explain the pore-fluid K isotope profiles at both sites. These slow-accumulating profiles are likely in diffusive steadystate, given that their characteristic time scales of diffusion $(\tau = L^2/2D)$, where D is diffusion rate corrected for temperature and tortuosity) are much shorter than the age of the sediments. That is, if we consider the deepest sediments at the slow-accumulating sites, τ values correspond to \sim 31 My at Site 1052 (sediment age = 121 Ma), and \sim 2 My at Site U1403 (sediment age = 77 Ma). Although any K-rich minerals formed at these sites are a trivial component of the global seawater K sink in marine sediments (e.g. Gieskes, 1981; Rudnicki et al., 2001), they are characterized by δ^{41} K values that are significantly lower than seawater. For example, at Sites 1052 and U1403 the predicted δ^{41} K values for hypothetical authigenic silicates associated with the deepest pore-fluids are -0.53 to -1.53% and -1.72to -2.72%, respectively, for α_{sink} of 1.0000–0.9990.

4.2. Potential mechanisms leading to K isotopic fractionation during reverse weathering and other K sink reactions

Model fits to measured δ^{41} K profiles are all improved by assuming that K-consuming reactions are accompanied by K isotopic fractionations ranging between 0.9980 and 1.0000. Evidence for the alteration of volcanic material at most sites suggests that secondary silicate formation is likely an important sink of pore-fluid K. Fractionation of K isotopes during incorporation into authigenic silicates

may arise from (1) equilibrium isotope effects associated with the diversity of K bonding environments in the mineral structure of phyllosilicates (Hill and Schauble, 2008; Bourg and Sposito, 2011; Underwood et al., 2016) and/or (2) rate-dependent kinetic isotope effects (DePaolo, 2011; Hofmann et al., 2012). Similar to other alkali and alkaliearth metals, equilibrium fractionation during partitioning of potassium isotopes between mineral and fluid phases is likely affected by changes in cation coordination number with the heavy isotope of an element tending to be enriched in the phase with the strongest bonds and lowest coordination numbers (Schauble, 2004; Wunder et al., 2007; Hill and Schauble, 2008). Aqueous K has a coordination number of 6 ± 2 (Glezakou et al., 2006; Varma and Rempe, 2006), while K in low-temperature clay minerals can have coordinations anywhere between 6 and 12 (Weiss et al., 1992; Cibin et al., 2005; Liu and Lu, 2006). The variability in coordination number of clay-bound K is related to both the clay mineral structure and the nature of the K complex formed. Upon adsorption onto clay surfaces, potassium may remain surrounded by water, forming outer-sphere complexes (OSC) with K coordination number similar to aqueous K (Meunier, 2005; Bourg and Sposito, 2011; Underwood et al., 2016). Alternatively, it may partially or fully dehydrate to form secondary and primary innersphere complexes (ISC), respectively (Meunier, 2005; Bourg and Sposito, 2011; Underwood et al., 2016). In the case of higher structural charge clays and mica, K strongly prefers to form inner-sphere complexes on exterior basal surfaces due to its relatively low solvation enthalpy (e.g. Lee et al., 2012; Bourg et al., 2017). Inner-sphere complexes contain K bonds with tetrahedral oxygen atoms, the number of which depends on the rotational angle of the tetrahedral sheet (Weiss et al., 1992; Cibin et al., 2005; Liu and Lu, 2006).

Under this structural framework, the incorporation of pore-fluid K into authigenic phyllosilicates may be accompanied by an increase in the K coordination number, leading to minerals that are enriched in 39K compared to the pore-fluid. This scenario is consistent with secondary mineral formation at Sites 1052, U1378 and U1395, where fractionation factors are estimated between 0.9980 and 0.9995. Alternatively, K coordination number might not change during K partitioning into low structural charge clay minerals such as montmorillonite, so that the δ^{41} K composition of the clay product resembles that of K in the fluid. This may explain the lack of K isotope fractionation estimated during K consumption at Site U1403. At this site, petrologic observations indicate the presence of authigenic montmorillonite, a swelling clay whose K-rich end-member can contain up to two layers of water in its interlayer space (Meunier, 2005) and interlayer cations can be fully hydrated (Hensen and Smit, 2002). Hence, estimated fractionation factor for Site U1403 ($\alpha_{sink} \sim 1.0000$) could be a result of K sorption as fully hydrated outer-sphere complexes (OSC) or partially hydrated inner-sphere complexes (ISC) on external basal sites and/or in the interlayer spaces of montmorillonite (Chang et al., 1998). The prediction that K sorption onto hydrous clays has an $\alpha_{sink} \sim 1.0000$ might also help explain (1) the seawater-like δ^{41} K composition of enriched pore-fluids at the sediment-water interface in U1403 and 1052, and (2) the smooth K isotopic profile for Site U1403 despite the noisy K concentration data (Fig. 2A and B). If we assume that sampling artifacts associated with sorption-desorption are responsible for these K enrichments and scatter (e.g. de Lange et al., 1992; Sacchi et al., 2001), we can speculate that these artifacts are caused by desorption of K from swelling clays with an $\alpha \sim 1.0000$, and that the clays sourcing K were in equilibrium with the pore-fluids.

The preferential removal of ³⁹K into K-rich minerals may also result from kinetic isotope effects. As previously discussed, K diffusion in aqueous solution can be associated with large kinetic isotope effects (0.9967–0.9984; Bourg et al., 2010), so that K delivery to the surface of growing clays via K diffusion through the pore-fluid may lead to ³⁹K enrichment of the clay product. K adsorption onto mineral surfaces can also lead to preferential incorporation of ³⁹K if it is accompanied by ion dehydration, as rates of ion desolvation increase with decreasing isotopic mass (Hofmann et al., 2012). This might be the case during K incorporation as inner-sphere complexes at the external surfaces of higher structural charge phyllosilicates (Lee et al., 2012; Bourg et al., 2017). In contrast, we do not expect kinetic fractionation from ion desolvation to be important when K is incorporated into anhydrous clay interlayers, as the rate-limiting step here is likely K penetration into the interlayer (Ruiz Pestana et al., 2016). The magnitude of K isotope effects due to desolvation is predicted to be between -2.0 and -2.8% ($\alpha = 0.9972-0.9980$; Hofmann et al., 2012), significantly larger than the range in α_{sink} values estimated in our models for secondary silicate formation (0.9980-1.0000). This difference may reflect the fact that K sink at all depths is a mixture of solvated $(\alpha_{sink} \sim 1.0000)$ and desolvated $(\alpha_{sink} \sim 0.9980)$ K. Alternatively, it may reflect a rate-dependence of the expression of the kinetic isotope effect associated with desolvation (DePaolo, 2011; Hofmann et al., 2012).

In summary, the removal of pore-fluid K into marine clays appears to be associated with little fractionation of K isotopes when the K does not undergo major changes in coordination number and/or remains hydrated (e.g. U1403). In contrast, when K desolvation is important or coordination number increases significantly during K uptake, ³⁹K is preferentially removed with estimated fractionation factors ranging from 0.9980 to 0.9995 (other sites). These values are smaller than but show the same directionality as MD predictions for the K isotope effects associated with ion desolvation reactions (Hofmann et al., 2012).

4.3. Ion-exchange reactions as a potential source of kinetic isotope effects in marine pore-fluids

NH₄⁺ produced during the decomposition of organic matter in sedimentary systems is capable of displacing K⁺ from clay interlayers through ion-exchange reactions (e.g. Boatman and Murray, 1982; Mackin and Aller, 1984; Breymann and Suess, 1988; James and Palmer, 2000). Two lines of evidence suggest that this phenomenon is

currently occurring at Sites U1378 and U1395. First, increases in NH₄⁺ concentrations associated with deflections/reversals in pore-fluid Mg and K profiles. Second, Mg isotope evidence, in particular from Site U1395, indicates a Mg source to the pore-fluid with a δ^{26} Mg value that is consistent with observations of exchangeable Mg in terrestrial systems (Wimpenny et al., 2014). Ion exchange also appears to be associated with light δ^{41} K values at Sites U1378 and U1395, suggesting that the potassium released during reaction has a low δ^{41} K value. Our calculated fractionation factors for local K-sourcing reactions at these sites are consistent with the preferential release of ³⁹K into the pore-fluid (ε_{source} <0).

Potassium released during cation exchange can be sourced from external basal sites, fraved-edge sites and/or interlayer sites. We have argued that adsorption onto montmorillonite, an expandable clay, is likely not associated with any significant isotope fractionation, as the reaction happens close to equilibrium. In contrast, in the case of non-swelling phyllosilicates (such as micas and illites), the energy barrier associated with potassium displacement from interlayer sites is significant (Ruiz Pestana et al., 2016) and these sites are generally regarded as nonexchangeable. However, NH₄ can still replace interlayer K⁺ because of its lower hydration energy (Teppen and Miller, 2006). As a result, K⁺ replacement by NH₄⁺ is favored with the potential for large kinetic isotope effects associated with diffusion-controlled transport of K out of the interlayer (Ruiz Pestana et al., 2016). If we assume that the equilibrium fractionation factor (α_{equil}) between anhydrous clay and solution is less than 1 (as discussed in 4.2), and that the forward fractionation factor (α_{forw}) is also less than 1 and likely smaller than α_{equil} (due to large enthalpy of reaction for K penetration into anhydrous interlayer sites; Ruiz Pestana et al., 2016), then the fractionation factor associated with the backward reaction (i.e. K release from the interlayer, α_{back}) must also be less than 1, since $\alpha_{equil} = \alpha_{forw}/\alpha_{back}$. This theoretical prediction for K isotope fractionation during ion exchange has the same directionality as our modeled isotope effects for local K source reactions at U1395 and U1378 ($\varepsilon_{source} < 0$ or $\alpha_{source} < 1$). Due to poor constraints on rates of reaction at these sites (i.e. R_{sink} , R_{source}), we are unable to give a meaningful range for these kinetic isotope effects; however, our models predict significantly large fractionations for cases when $R_{sink} \gg R_{source}$ (Fig. 7). In contrast, for cases when $\varepsilon_{source} \sim 0$ (meters 28–46 at Site U1378 when $R_{sink} \ll R_{source}$; Fig. 7), we suggest that these might be associated with ion-exchange reactions that happen close to equilibrium, i.e. exchanged K is sourced from the external basal surface or interlayer sites of swelling clays (readily exchangeable K).

4.4. The significance of deep-sea sedimentary environments for understanding the global potassium cycle

Assuming a global K cycle in seawater that is close to steady-state (residence time $\sim 10^7$ years; Broecker and Peng, 1982), the high δ^{41} K value of seawater must reflect

K isotope fractionation during either the formation of (1) clays associated with silicate weathering on the continents, (2) secondary Al-silicates associated with K removal in marine sediments (Michalopoulos and Aller, 1995; Hover et al., 2002) and low-temperature hydrothermal systems (Bloch and Bischoff, 1979; Hover et al., 2002; Holland, 2005; Parendo et al., 2017), or (3) some combination of the two. In this study, we address potential K isotopic fractionation associated with K removal in deep-sea marine sediments.

Although deep-sea sedimentary systems do not constitute a major sink of seawater K (e.g. Gieskes, 1981: Rudnicki et al., 2001), these sites yield important constraints on the processes responsible for fractionating K isotopes during marine reverse silicate weathering. Our results provide the first evidence that marine clays preferentially incorporate ³⁹K and suggest three potential mechanisms: (1) K supply to the surfaces of growing clays by K diffusion down concentration gradients, (2) equilibrium isotope effects associated with changes in K coordination number upon incorporation by authigenic Al-silicates, and (3) kinetic isotope effects related to rates of mineral precipitation. Although K isotope effects due to diffusion requires large concentration gradients, these have been observed in shallow-water systems that are thought to constitute globally significant sinks of seawater K (Michalopoulos and Aller, 1995; Hover et al., 2002; Cuadros et al., 2017). In addition, our model results, particularly those for the rapidly accumulating Sites U1378 and U1395, indicate that K removal into marine clays may also be accompanied by fractionation of K isotopes. The magnitude of this isotope effect appears to vary depending on the extent to which K undergoes changes in coordination number and desolvation during incorporation into the marine clay. Overall, the isotope effects predicted here appear to be sufficient to explain, in part, the high δ^{41} K value of seawater relative to bulk silicate Earth.

Finally, K cycling in natural marine sediments likely involves a wide range of substrates composed of a number of different phyllosilicate and zeolite minerals and modeled fractionation factors need not be unique. Rather, they might reflect the composition of K released from or taken up by different silicate minerals, with each individual monominerallic reaction having its own isotopic expression. Further studies will be needed under controlled conditions to tease these mineral and rate-dependent effects apart. However, the good agreement between model results and the pore-fluid profiles using a similar set of boundary conditions and fractionation factors for each site indicates that the K isotopic effects observed here are likely broadly applicable to K removal by marine Al-silicate authigenesis.

5. CONCLUSIONS

It has recently been recognized that potassium in seawater ($\delta^{41}K \sim 0\%$) and bulk silicate Earth ($\delta^{41}K \sim -0.54\%$) are isotopically distinct (Li et al., 2016; Wang and Jacobsen, 2016; Morgan et al., 2018), although little is known about the mechanisms responsible for this difference (Parendo et al., 2017). Considered in the context of the

global geochemical cycle of K in seawater, the difference in δ^{41} K values between seawater and BSE implies that either 39 K is preferentially retained by terrestrial clays during continental silicate weathering, or that 39 K is preferentially removed from seawater during the formation of authigenic Al-silicates in marine sediments and altered oceanic crust, or some combination of the two. To constrain K isotope fractionation during marine reverse silicate weathering, we measured deep-sea sediment pore-fluids from four IODP/ODP sites all of which are characterized by reactions that consume pore-fluid K within the sediment column and/or in the underlying crust but which differ in average sedimentation rate and lithology.

We find that pore-fluid profiles of δ^{41} K values from slow-accumulating sites are mainly controlled by K fractionation during diffusion, whereas in rapidly accumulating sites diffusion and fractionation associated with reaction (e.g. secondary Al-silicate formation and ion exchange with NH₄) may all play important roles in determining the porefluid δ^{41} K profiles. Using a 1D model of the sediment porefluid system, we show that K isotope fractionation factors associated with diffusion of K in marine sedimentary systems agree with experiments and molecular dynamic simulations of aqueous K diffusion (Bourg et al., 2010) and give a best estimate of $0.9967 \leqslant \alpha_{diff} \leqslant 0.9974$. Model simulations of all four sites are consistent with K isotope fractionation factors between 0.9980 and 1.0000 for lowtemperature marine silicate reverse weathering. We argue that this range of fractionation values might result from (1) equilibrium isotope effects associated with variable coordination states of potassium in clay minerals and/or (2) kinetic isotope effects related to rates of clay authigenesis and K desolvation during incorporation into external surfaces of higher structural charge phyllosilicates. Our results also show that local ion exchange reactions in marine sediments (e.g. K release from clays in exchange with porefluid NH₄) may be associated with large kinetic isotope effects ($\alpha \le 1.0000$) when the K is sourced from the interlayers of non-swelling clays (e.g. illites). Finally, we propose that K desorption ($\alpha \sim 1.0000$) from external basal sites or interlayers of swelling clays during pore-fluid sampling and/or fluid extraction from sediments (e.g. by squeezing) is likely responsible for the K enrichment reported for shallow pore-fluids (1052, U1403) and the concentration scatter at U1403 (Mangelsdorf et al., 1969; Sayles and Manheim, 1975; de Lange et al., 1992; Sacchi et al., 2001). However, such enrichment does not appear to affect pore-fluid δ^{41} K values when the sediments are in equilibrium with the fluid

Although the sites studied here constitute only a small fraction of the global K sink in marine authigenic silicates, the processes that determine deep-sea pore-fluid δ^{41} K profiles also operate in shallow-water systems, where most marine authigenic Al-silicate formation occurs. We speculate that both diffusion and reverse silicate weathering reactions fractionate K isotopes in these systems and that together these effects result in an authigenic marine clay sink enriched in 39 K. As preliminary measurements of the δ^{41} K value of hydrothermally altered oceanic crust indicate

that this processes appears to incorporate K that is not fractionated relative to seawater (Parendo et al., 2017), fractionation of K isotopes during sedimentary marine reverse weathering likely plays an important role in raising the δ^{41} K value of seawater above the bulk silicate Earth value.

ACKNOWLEDGMENTS

The authors would like to thank Ian C. Bourg for his invaluable insights on the kinetics of cation exchange and K complexation in clay minerals, Satish C.B. Myneni for discussions on clay mineral structure, and Elizabeth Lundstrom for the experimental data on Ca fractionation discussed in Section 2.5.3. Reviews by Dr. L. Coogan and Dr. L. Lammers are also greatly appreciated and significantly improved this manuscript. All pore-fluid samples used in this study were sourced by the Ocean Drilling Program (ODP) and the Integrated Ocean Drilling Program (IODP). This work was funded through NSF OCE CAREER grant #1654571 to J. A. Higgins. Any use of trade, product, or firm names is for descriptive purposes only and does not imply endorsement by the U.S. Government.

APPENDIX A. SUPPLEMENTARY MATERIAL

Supplementary data associated with this article can be found, in the online version, at https://doi.org/10.1016/j.gca.2018.02.035.

REFERENCES

- Archer D. (1991) Equatorial Pacific calcite preservation cycles: production or dissolution? *Paleoceanography* 6, 561–571.
- Berner R. A. (1980) Early Diagenesis: A Theoretical Approach.
 Princeton University Press, Princeton, NJ.
- Berner R. A., Lasaga A. C. and Garrels R. M. (1983) The carbonate-silicate geochemical cycle and its effect on the atmospheric carbon dioxide over the past 100 million years. *Am. J. Sci.* **283**, 641–683.
- Blättler C. L., Miller N. R. and Higgins J. A. (2015) Mg and Ca isotope signatures of authigenic dolomite in siliceous deep-sea sediments. *Earth Planet. Sci. Lett.* **419**, 32–42.
- Bloch S. and Bischoff J. L. (1979) The effect of low-temperature alteration of basalt on the oceanic budget of potassium. *Geology* 7, 193–196.
- Boatman C. D. and Murray J. W. (1982) Modeling exchangeable NH₄⁺ adsorption in marine sediments: process and controls of adsorption. *Limnol. Oceanogr.* 27, 99–110.
- Boudreau B. P. (1997) Diagenetic Models and Their Implementation: Modelling Transport and Reactions in Aquatic Sediments. Springer-Verlag, New York.
- Bourg I. and Sposito G. (2011) Ion exchange phenomena. In *Handbook of Soil Science* (ed. M. E. Sumner). CRC Press, Boca Raton, FL, p. 16.
- Bourg I. C., Lee S. S., Fenter P. and Tournassat C. (2017) Stern layer structure and energetics at mica–water interfaces. *J. Phys. Chem. C* 121, 9402–9412.
- Bourg I. C., Richter F. M., Christensen J. N. and Sposito G. (2010) Isotopic mass dependence of metal cation diffusion coefficients in liquid water. *Geochim. Cosmochim. Acta* 74, 2249–2256.
- Breymann M. T. V. and Suess E. (1988) Magnesium in the marine sedimentary environment: Mg-NH₄ ion exchange. *Chem. Geol.* **70**, 359–371.

- Broecker W. S. and Peng T. H. (1982) Tracers in the Sea. Lamont-Doherty Geological Observatory, Columbia University, Palisades, New York.
- Bryant C., McCulloch M. and Bennett V. (2003) Impact of matrix effects on the accurate measurement of Li isotope ratios by inductively coupled plasma mass spectrometry (MC-ICP-MS) under "cold" plasma conditions. *J. Anal. Atom. Spectrom.* 18, 734–737.
- Chang F. R. C., Skipper N. and Sposito G. (1998) Monte Carlo and molecular dynamics simulations of electrical double-layer structure in potassium- montmorillonite hydrates. *Langmuir* 14, 1201–1207
- Cibin G., Mottana A., Marcelli A. and Brigatti M. (2005) Potassium coordination in trioctahedral micas investigated by K-edge XANES spectroscopy. *Mineral. Petrol.* **85**, 67–87.
- Coogan L. A. and Gillis K. M. (2013) Evidence that low-temperature oceanic hydrothermal systems play an important role in the silicate-carbonate weathering cycle and long-term climate regulation. *Geochem. Geophys. Geosyst.* 14, 1771–1786.
- Cuadros J., Andrade G., Ferreira T. O., de Moya Partiti C. S., Cohen R. and Vidal-Torrado P. (2017) The mangrove reactor: fast clay transformation and potassium sink. *Appl. Clay Sci.* 140, 50–58.
- Demicco R. V., Lowenstein T. K., Hardie L. A. and Spencer R. J. (2005) Model of seawater composition for the Phanerozoic. *Geology* 33, 877–880.
- DePaolo D. J. (2011) Surface kinetic model for isotopic and trace element fractionation during precipitation of calcite from aqueous solutions. Geochim. Cosmochim. Acta 75, 1039– 1056
- Dunlea A. G., Murray R. W., Santiago Ramos D. P. and Higgins J. A. (2017) Cenozoic global cooling and increased seawater Mg/Ca via reduced reverse weathering. *Nature Commun.* 8, 7. https://doi.org/10.1038/s41467-017-00853-5.
- Elderfield H., Wheat C., Mottl M., Monnin C. and Spiro B. (1999)
 Fluid and geochemical transport through oceanic crust: a transect across the eastern flank of the Juan de Fuca Ridge. *Earth Planet. Sci. Lett.* **172**, 151–165.
- Fantle M. S. and Higgins J. (2014) The effects of diagenesis and dolomitization on Ca and Mg isotopes in marine platform carbonates: implications for the geochemical cycles of Ca and Mg. *Geochim. Cosmochim. Acta* 142, 458–481.
- Galy A., Belshaw N. S., Halicz L. and O'Nions R. K. (2001) Highprecision measurement of magnesium isotopes by multiplecollector inductively coupled plasma mass spectrometry. *Int. J. Mass Spectrom.* 208, 89–98.
- Gieskes J. M. (1975) Chemistry of interstitial waters of marine sediments. *Ann. Rev. Earth Planet. Sci.* **3**, 433–453. https://doi.org/10.1146/annurev.ea.03.050175.002245.
- Gieskes J. M. (1981) Deep-sea drilling interstitial water studies: implications for chemical alteration of the oceanic crust, layers I and II. *Special Publ. SEPM* **32**, 149–167.
- Glezakou V. A., Chen Y., Fulton J. L., Schenter G. K. and Dang L. X. (2006) Electronic structure, statistical mechanical simulations, and EXAFS spectroscopy of aqueous potassium. *Theor. Chem. Acc.: Theory Comput. Model. (Theor. Chim.* Acta) 115, 86–99.
- Hensen E. J. and Smit B. (2002) Why clays swell. *J. Phys. Chem. B* **106**, 12664–12667.
- Higgins J. A. and Schrag D. P. (2010) Constraining magnesium cycling in marine sediments using magnesium isotopes. *Geochim. Cosmochim. Acta* **74**, 5039–5053.
- Higgins J. A. and Schrag D. P. (2015) The Mg isotopic composition of Cenozoic seawater–evidence for a link between Mg-clays, seawater Mg/Ca, and climate. *Earth Planet. Sci. Lett.* 416, 73–81.

- Hill P. S. and Schauble E. A. (2008) Modeling the effects of bond environment on equilibrium iron isotope fractionation in ferric aquo-chloro complexes. *Geochim. Cosmochim. Acta* 72, 1939– 1958.
- Hofmann A. E., Bourg I. C. and DePaolo D. J. (2012) Ion desolvation as a mechanism for kinetic isotope fractionation in aqueous systems. *Proc. Natl. Acad. Sci.* 109, 18689–18694. https://doi.org/10.1073/pnas.1208184109.
- Holland H. D. (2005) Sea level, sediments and the composition of seawater. Am. J. Sci. 305, 220–239.
- Horita J., Zimmermann H. and Holland H. D. (2002) Chemical evolution of seawater during the Phanerozoic: implications from the record of marine evaporites. *Geochim. Cosmochim.* Acta 66, 3733–3756.
- Hover V., Walter L. and Peacor D. (2002) K uptake by modern estuarine sediments during early marine diagenesis, Mississippi Delta Plain, Louisiana, USA. *J. Sediment. Res.* **72**, 775–792.
- Husson J. M., Higgins J. A., Maloof A. C. and Schoene B. (2015) Ca and Mg isotope constraints on the origin of Earth's deepest δ^{13} C excursion. *Geochim. Cosmochim. Acta* **160**, 243–266.
- James R. H. and Palmer M. R. (2000) Marine geochemical cycles of the alkali elements and boron: the role of sediments. *Geochim. Cosmochim. Acta* 64, 3111–3122.
- Kronberg B. (1985) Weathering dynamics and geosphere mixing with reference to the potassium cycle. *Phys. Earth Planet. Inter.* 41, 125–132.
- de Lange G., Cranston R., Hydes D. and Boust D. (1992) Extraction of pore water from marine sediments: a review of possible artifacts with pertinent examples from the North Atlantic. *Marine Geol.* **109**, 53–76.
- Le Friant, A., Ishizuka, O., Stroncik, N., Slagle, A., et al. (2013). Site U1395. In Proceedings of the Integrated Ocean Drilling Program, 340, Integrated Ocean Drilling Program Management International, Inc., Tokyo. p. 59.
- Lee S. S., Fenter P., Nagy K. L. and Sturchio N. C. (2012) Monovalent ion adsorption at the muscovite (001)–solution interface: relationships among ion coverage and speciation, interfacial water structure, and substrate relaxation. *Langmuir* 28, 8637–8650.
- Li W., Beard B. L. and Li S. (2016) Precise measurement of stable potassium isotope ratios using a single focusing collision cell multi-collector ICP-MS. *J. Anal. Atom. Spectrom.* **31**, 1023–1020
- Liu X. D. and Lu X. C. (2006) A thermodynamic understanding of clay-swelling inhibition by potassium ions. *Angew. Chem. Int. Ed.* **45**, 6300–6303.
- Lowenstein T. K., Timofeeff M. N., Brennan S. T., Hardie L. A. and Demicco R. V. (2001) Oscillations in Phanerozoic seawater chemistry: evidence from fluid inclusions. *Science* 294, 1086– 1088.
- Mackenzie F. T. and Garrels R. M. (1966) Chemical mass balance between rivers and oceans. *Am. J. Sci.* **264**, 507–525.
- Mackin J. E. and Aller R. C. (1984) Ammonium adsorption in marine sediments. *Limnol. Oceanogr.* 29, 250–257.
- Manga M., Hornbach M. J., Le Friant A., Ishizuka O., Stroncik N., Adachi T., Aljahdali M., Boudon G., Breitkreuz C. and Fraass A., et al. (2012) Heat flow in the Lesser Antilles island arc and adjacent back arc Grenada basin. *Geochem. Geophys. Geosyst.* 13, 19.
- Mangelsdorf P., Wilson T. and Daniell E. (1969) Potassium enrichments in interstitial waters of recent marine sediments. *Science* **165**, 171–174.
- McDuff R. E. (1981) Major cation gradients in DSDP interstitial waters: the role of diffusive exchange between seawater and upper oceanic crust. *Geochim. Cosmochim. Acta* **45**, 1705–1713.

- Meunier A. (2005) *Clays*. Springer Science & Business Media, Berlin.
- Michalopoulos P. and Aller R. C. (2004) Early diagenesis of biogenic silica in the Amazon delta: alteration, authigenic clay formation, and storage. *Geochim. Cosmochim. Acta* 68, 1061– 1085
- Michalopoulos P. and Aller R. C., et al. (1995) Rapid clay mineral formation in Amazon Delta sediments: reverse weathering and oceanic elemental cycles. *Science* **270**, 614–617.
- Morgan, L. E., Santiago Ramos, D. P., Lloyd, N. S. and Higgins, J. A. (2018). High precision $^{41}\text{K}/^{39}\text{K}$ measurements by MC-ICP-MS indicate terrestrial variability of $\delta^{41}\text{K}$. J. Anal. Atom. Spectrom. doi:https://doi.org/10.1039/C7JA00257B.
- Norris, R., Kroon, D., Klaus, A., et al. (1998a). Site 1052. In Proceedings of the Ocean Drilling Program, Initial Reports 171B, Ocean Drilling Program, College Station, TX. pp. 241–319.
- Norris, R., Kroon, D., Klaus, A., et al. (1998b). Site 1053. In Proceedings of the Ocean Drilling Program, Initial Reports 171B, Ocean Drilling Program, College Station, TX. pp. 321–348.
- Norris, R., Wilson, P., Blum, P., et al. (2014a). Site U1403. In Proceedings of the Integrated Ocean Drilling Program, 342, Integrated Ocean Drilling Program, College Station, TX. p. 98.
- Norris, R., Wilson, P., Blum, P., et al. (2014b). Site U1405. In Proceedings of the Integrated Ocean Drilling Program, 342, Integrated Ocean Drilling Program, College Station, TX. p. 95.
- Parendo C. A., Jacobsen S. B. and Wang K. (2017) K isotopes as a tracer of seafloor hydrothermal alteration. *Proc. Natl. Acad. Sci.* **114**, 1827–1831.
- Pearson C. E. (1968) On a differential equation of boundary layer type Stud. Appl. Math. 47, 134–154.
- Richter F. M. and DePaolo D. J. (1987) Numerical models for diagenesis and the Neogene Sr isotopic evolution of seawater from DSDP Site 590B. Earth Planet. Sci. Lett. 83, 27–38.
- Richter F. M. and DePaolo D. J. (1988) Diagenesis and Sr isotopic evolution of seawater using data from DSDP 590B and 575. *Earth Planet. Sci. Lett.* **90**, 382–394.
- Ross, N., Torres, M. E., Haley, B. A., Solomon, E. A. and Kastner, M. (2015). Data report: strontium isotope analyses of pore fluids from the CRISP-A transect drilled during Expeditions 334 and 344. In Proceedings of the Integrated Ocean Drilling Program, 344, Integrated Ocean Drilling Program, College Station, TX. p. 13.
- Rudnicki M. D., Wilson P. A. and Anderson W. T. (2001) Numerical models of diagenesis, sediment properties, and pore fluid chemistry on a paleoceanographic transect: Blake Nose, Ocean Drilling Program Leg 171B. *Paleoceanography* 16, 563– 575
- Ruiz Pestana L., Kolluri K., Head-Gordon T. and Lammers L. N. (2016) Direct exchange mechanism for interlayer ions in nonswelling clays. *Environ. Sci. Technol.* 51, 393–400.
- Sacchi E., Michelot J. L., Pitsch H., Lalieux P. and Aranyossy J. F. (2001) Extraction of water and solutes from argillaceous rocks for geochemical characterisation: methods, processes and current understanding. *Hydrogeol. J.* 9, 17–33.
- Sayles F. L. and Manheim F. T. (1975) Interstitial solutions and diagenesis in deeply buried marine sediments: results from the Deep Sea Drilling Project. *Geochim. Cosmochim. Acta* 39, 103– 127.
- Schauble E. A. (2004) Applying stable isotope fractionation theory to new systems. *Rev. Mineral. Geochem.* **55**, 65–111.
- Spencer R. and Hardie L. (1990) Control of seawater composition by mixing of river waters and mid-ocean ridge hydrothermal brines. Geochem. Soc. Special Publ. 2. Geochem. Soc. Special Publ. 2, 409–449.

- Staudigel H. and Hart S. R. (1983) Alteration of basaltic glass: mechanisms and significance for the oceanic crust-seawater budget. Geochim. Cosmochim. Acta 47, 337–350.
- Teppen B. J. and Miller D. M. (2006) Hydration energy determines isovalent cation exchange selectivity by clay minerals. Soil Sci. Soc. Am. J. 70, 31–40.
- Tipper E. T., Louvat P., Capmas F., Galy A. and Gaillardet J. (2008) Accuracy of stable Mg and Ca isotope data obtained by MC-ICP-MS using the standard addition method. *Chem. Geol.* **257** 65–75
- Underwood T., Erastova V. and Greenwell H. C. (2016) Ion adsorption at clay-Mineral surfaces: the Hofmeister series for hydrated smectite minerals. Clays Clay Min. 64, 472–487.
- Vannucchi, P., Ujiie, K., Stroncik, N., Malinverno, A., et al. (2012). Site U1378. In Proceedings of the Integrated Ocean Drilling Program, 334, Integrated Ocean Drilling Program Management International, Inc., Tokyo. p. 62.
- Varma S. and Rempe S. B. (2006) Coordination numbers of alkali metal ions in aqueous solutions. *Biophys. Chem.* 124, 192–199.
- Walker J., Hays P. and Kasting J. (1981) A negative feedback mechanism for the long-term stabilization of Earth's surface temperature. J. Geophys. Res.-Oceans Atmosph. 86, 9776–9782.
- Wang K. and Jacobsen S. B. (2016) An estimate of the Bulk Silicate Earth potassium isotopic composition based on MC-ICPMS measurements of basalts. *Geochim. Cosmochim. Acta* 178, 223–232.

- Weiss Z., Rieder M. and Chmielova M. (1992) Deformation of coordination polyhedra and their sheets in phyllosilicates. *Euro*. J. Mineral. 4, 665–682.
- Wheat C. G. and Mottl M. J. (2000) Composition of pore and spring waters from Baby Bare: global implications of geochemical fluxes from a ridge flank hydrothermal system. *Geochim. Cosmochim. Acta* **64**, 629–642.
- Wimpenny J., Colla C. A., Yin Q. Z., Rustad J. R. and Casey W. H. (2014) Investigating the behaviour of Mg isotopes during the formation of clay minerals. *Geochim. Cosmochim. Acta* 128, 178–194.
- Wunder B., Meixner A., Romer R. L., Feenstra A., Schettler G. and Heinrich W. (2007) Lithium isotope fractionation between Li-bearing staurolite, Li-mica and aqueous fluids: an experimental study. *Chem. Geol.* 238, 277–290.
- Young E. D. and Galy A. (2004) The isotope geochemistry and cosmochemistry of magnesium. Rev. Mineral. Geochem. 55, 197–230.
- Yuan-Hui L. and Gregory S. (1974) Diffusion of ions in sea water and in deep-sea sediments. *Geochim. Cosmochim. Acta* **38**, 703–714.

Associate editor: Thomas M. Marchitto

